The Astrophysical Journal, 740:65 (18pp), 2011 October 20 doi:10.1088/0004-637X/740/2/65

A VERY LARGE ARRAY SEARCH FOR 5 GHz RADIO TRANSIENTS AND VARIABLES AT LOW GALACTIC LATITUDES

E. O. Ofek[1,7], D. A. Frail[2], B. Breslauer[2,3], S. R. Kulkarni[1], P. Chandra[4], A. Gal-Yam[5], M. M. Kasliwal[1], and N. Gehrels[6]

[1] Division of Physics, Mathematics and Astronomy, California Institute of Technology, Pasadena, CA 91125, USA
[2] National Radio Astronomy Observatory, P.O. Box 0, Socorro, NM 87801, USA
[3] Department of Physics and Astronomy, Oberlin College, Oberlin, OH 44074-1088, USA
[4] Department of Physics, Royal Military College of Canada, Kingston, ON, Canada
[5] Benoziyo Center for Astrophysics, Weizmann Institute of Science, 76100 Rehovot, Israel
[6] NASA-Goddard Space Flight Center, Greenbelt, MD 20771, USA
Received 2011 March 11; accepted 2011 July 18; published 2011 September 30

ABSTRACT

We present the results of a 5 GHz survey with the Very Large Array (VLA) and the expanded VLA, designed to search for short-lived ($\lesssim$1 day) transients and to characterize the variability of radio sources at milli-Jansky levels. A total sky area of 2.66 deg^2, spread over 141 fields at low Galactic latitudes ($b \cong$ 6–8 deg), was observed 16 times with a cadence that was chosen to sample timescales of days, months, and years. Most of the data were reduced, analyzed, and searched for transients in near real-time. Interesting candidates were followed up using visible light telescopes (typical delays of 1–2 hr) and the X-ray Telescope on board the *Swift* satellite. The final processing of the data revealed a single possible transient with a peak flux density of $f_\nu \cong 2.4$ mJy. This implies a transient's sky surface density of $\kappa(f_\nu > 1.8\,\mathrm{mJy}) = 0.039^{+0.13,+0.18}_{-0.032,-0.038}$ deg^{-2} (1σ, 2σ confidence errors). This areal density is roughly consistent with the sky surface density of transients from the Bower et al. survey extrapolated to 1.8 mJy. Our observed transient areal density is consistent with a neutron star's origin for these events. Furthermore, we use the data to measure the source variability on timescales of days to years, and we present the variability structure function of 5 GHz sources. The mean structure function shows a fast increase on $\approx$1 day timescale, followed by a slower increase on timescales of up to 10 days. On timescales between 10 and 60 days, the structure function is roughly constant. We find that $\gtrsim$30% of the unresolved sources brighter than 1.8 mJy are variables at the $>4\sigma$ confidence level, presumably mainly due to refractive scintillation.

Key words: radio continuum: general – stars: neutron – techniques: photometric

Online-only material: color figures, machine-readable tables

1. INTRODUCTION

Radio surveys of the sky in the time domain have often been used to identify new astrophysical phenomena. Highly variable radio sources can serve as signposts to compact, high-energy objects which are accompanied by high magnetic fields and/or relativistic particle acceleration. Radio variability from quasars and γ-ray bursts (Dent 1965; Frail et al. 1997) was used to infer bulk relativistic motions in these objects (Rees 1967; Goodman et al. 1987). Notable new phenomena identified from radio time-domain surveys include the discovery of the first pulsars (Hewish et al. 1968), the Galactic high-energy binary LSI+61°303 (Gregory & Taylor 1978), the anomalous variability of 4C 21.53 that led to the discovery of millisecond pulsars (Backer et al. 1982), and the still-mysterious extreme scattering events (Fiedler et al. 1987).

More recent surveys have found several new types of radio transients whose identity has remained unknown or not well understood (e.g., Hyman et al. 2005; McLaughlin et al. 2006; Bower et al. 2007; Lorimer et al. 2007; Niinuma et al. 2007; Kida et al. 2008; Matsumura et al. 2009).

Specifically, Bower et al. (2007) reanalyzed 944 epochs of Very Large Array[8] (VLA) observations, taken about once per week for 22 years, of a single calibration field. These authors discovered a total of ten transients, eight in the 5 GHz band and two in the 8 GHz band. Eight of these transients were detected in a single epoch. Therefore, their duration is shorter than the time between successive epochs (one week) and longer than the exposure time (20 minutes). Moreover, the majority of these sources do not have any optical counterpart coinciding with their position. The lack of optical counterparts down to limiting magnitudes of 27.6 in the g band and 26.5 in the R band is especially puzzling and significantly limits the classes of objects that can be associated with these events (Ofek et al. 2010).

Kuniyoshi et al. (2006), Niinuma et al. (2007), and Kida et al. (2008) reported a search for radio transients using an east–west interferometer of the Nasu Pulsar Observatory (located in Tochigi Prefecture, Japan) of Waseda University. To date, this program reported 11 bright radio transients with peak flux densities above 1 Jy in the 1.4 GHz band.

Recently, in Ofek et al. (2010) we suggested that the properties of the single-epoch "Bower et al. transients" and the Nasu transients are consistent with emerging from a single class of objects, namely, isolated old neutron stars (NS). Specifically, the NS hypothesis is consistent with the rate, energetics, sky surface density, source number count function, and the lack of optical counterparts.

In this paper, we present a new VLA survey for radio transients and variables at low Galactic latitudes. Our main motivation for this survey was to detect short-lived radio transients,

[7] Einstein fellow.
[8] The Very Large Array is operated by the National Radio Astronomy Observatory (NRAO), a facility of the National Science Foundation operated under cooperative agreement by Associated Universities, Inc.

Table 1
Previous GHz Transient and Variability Surveys

ν (GHz)	Area (deg^2)	Direction (deg)	$\Delta\theta$ ($''$)	$N_{\rm ep}$	δt	Δt	rms (mJy)	Sources	Tran.	Var.	Reference
0.84	2776	$\delta < -30$	$\sim$45	2[a]	12 hr	1 day–20 yr	2.8	29730	2	$\sim$10	14
1.4	0.22	$l = 150, b = +53$	4.5	3	6 hr	19 days, 17 months	0.015	...	0	2%	1
1.4	2.6	$l = 151, b = +24$	60	16	12 hr	1–12 days, 1–3 months	0.7	245	0	$\sim$1%	2
1.4	120	South Galactic cap	5	2	days	7 yr	0.15	9086	0	1.4%	3
1.4	2500	$b \gtrsim 30$	45	2	days	$\sim$years	0.45	7181	1	...	5–7
1.4	2870[b]	$+32 > \delta > +42$	$24' \times 2.'4$	$\sim$1000	4 min	1 day	300	...	11	...	8–11
1.4	0.2	$l = 57, b = +81$	20	1852	minutes	1 day–23 yr	2	10	0	...	19
1.4	690	$l = 70, b = +64$	150	2	months	15 yr	3.94	4408	0	$\sim$0.1%	4
1.4	690	$l = 70, b = +64$	150	12	>1 day	days–months	38	4408	0	$\lesssim$0.5%	20
1.4	0.2	Phase calibration	...	151	5 min	days–years	$\sim$1	...	0	...	21
3.1	10	$l = 57, b = +67$	100	2	months	15 yr	0.25	425	1[c]	...	12
4.9	0.1	Phase calibration	...	$\sim$390[d]	5 min	days–years	$\sim$1	...	0	...	21
4.9	0.69	Extragalactic	0.5–15	2	60 min	1–100 days	0.05	...	0	...	15
4.9	23.2	$\lvert b\rvert < 0.4$	5	3	90 s	2 months–15 yr	0.2	2700	0	15	16
4.9	500	$\lvert b\rvert < 2$	180	16	2 min	1 day–5 yr	4.6	1274	1	$\sim$0.5	18
4.9	19924	$75 > \delta > 0$	210	2	$\sim$week	1 yr	5	75162	0	>40	17
4.9	0.07	$l = 115, b = +36$	5	626	20 min	1 week–22 yr	0.05	8	7[e]	0	13
8.5	0.02	$l = 115, b = +36$	3	599	20 min	1 week–22y	0.05	4	1[e]	0	13
8.5	0.04	Phase calibration	...	$\sim$308[f]	5 min	days–years	$\sim$1	...	0	...	21
4.9	2.6	$\lvert b\rvert \approx 7$	15	16	50 s	1 day–2 yr	0.15	$\sim$200	1	0.3%–30%	This paper

Notes. Columns description: $\Delta\theta$ is the beam full width at half-power; $N_{\rm ep}$ is the number of epochs; δt is the time span over which each epoch was obtained (see the text); Δt is the range of time separations between epochs; Sources is the number of persistent sources detected; Tran. is the number of transients found by the survey; Var. is the number or percentage of variables showing variability larger than 50%. We note that strong variables are defined differently by each survey. Therefore, these numbers provide only a qualitative comparison between the surveys.

[a] Smaller fraction of the sky was observed more than twice.

[b] The total surveyed area is about 2870 deg^2, but about 460 deg^2 was surveyed every day. These parameters are deduced from Kida et al. (2008) and Matsumura et al. (2009) (see Section 2).

[c] Marginal detection (4.3σ). Ignored in Figure 1.

[d] Mean number of epochs per field. Seven fields were observed on 2732 epochs.

[e] In addition, one transient was found by combining two months worth of data and no transients were found by combining 1 yr worth of data.

[f] Mean number of epochs per field. Seven fields were observed on 2154 epochs.

References. (1) Carilli et al. 2003; (2) Frail et al. 1994; (3) de Vries et al. 2004; (4) Croft et al. 2010; (5) Levinson et al. 2002; (6) Gal-Yam et al. 2006; (7) Ofek et al. 2010; (8) Matsumura et al. 2009; (9) Kida et al. 2008; (10) Kuniyoshi et al. 2006; (11) Matsumura et al. 2007; (12) Bower et al. 2010; (13) Bower et al. 2007; (14) Bannister et al. 2011; (15) Frail et al. 2003; (16) Becker et al. 2010; (17) Scott 1996; (18) Gregory & Taylor 1986; (19) Bower & Saul 2011; (20) Croft et al. 2011; (21) Bell et al. 2011.

with the goal of identifying them in real-time in order to find their counterparts at other wavelengths for further study. A second and equally important motivation for this survey was to characterize the transient and variable radio sky with a sensitivity and cadence that had not been carried out previously.

The organization of this paper is as follows. In Section 2 we provide a summary of previous radio transient and variability surveys. In Section 3 we present the observations, while the data reduction is outlined in Section 4. The results from our real-time transients search are provided in Section 5. Section 6 presents the source catalogs generated in the post-survey phase. The final post-survey transient search is described in Section 7, while a study of the sources variability is presented in Section 8. The implications of this study are discussed in Section 9 and we summarize in Section 10. In addition, three appendices discussing flux calibration, the statistics of max/min of a time series, and transient areal density calculation in the case of a beam with non-uniform sensitivity are provided.

2. PREVIOUS GHz SURVEYS FOR TRANSIENTS AND VARIABLES

Existing 0.8–8 GHz surveys have already explored, to some extent, the dynamic radio sky with a wide range of sensitivities, angular resolution, and cadences. However, compared with synoptic surveys at higher frequencies (infrared to γ-rays) the radio sky remains poorly explored. In Table 1 we summarize past synoptic radio surveys. We note that this summary includes only surveys looking for "slow" transients, where slow refers to events in which the pulse dispersion is not important. For each survey we also list the number of transients, as well as variables which vary by more than 50%. We note, however, that comparison of these numbers is complicated due to several factors. A radio image may be accomplished either through a single pointing or adding several scans taken at different times. If the time span, δt, containing all the observations composing a single "epoch" is larger than the transient duration (or variability timescale) then the survey sensitivity to transients (variables) is degraded. Additionally, the probability of detecting significant variability depends on δt and the typical timescale between epochs (Δt), through the variability structure function. Depending on the statistical method used to define the variability amplitude, it may be affected by the number of epochs ($N_{\rm ep}$) in the survey.

Here we provide a summary of some of the sky surveys listed in Table 1.

2.1. Surveys at Frequencies below 2 GHz

Carilli et al. (2003) used a deep, single VLA pointing at 1.4 GHz toward the Lockman hole. They found that only a

small fraction, $\leqslant 2\%$, of radio sources above a peak flux density limit of 0.1 mJy are highly (>50%) variable on 19 day and 17 month timescales. No transients were identified. Frail et al. (1994) imaged a much larger field at 1.4 GHz toward a γ-ray burst with the Dominion Radio Astrophysical Observatory synthesis telescope, making daily measurements for two weeks and then on several single epochs for up to three months. No transients were identified on these timescales, and no sources above a peak flux density limit of 3.5 mJy were seen to vary by more than 4σ.

There have also been a number of wide field surveys of the sky at 1.4 GHz. de Vries et al. (2004) used the VLA to image a region, toward the South Galactic cap, twice on a seven-year timescale. No transients were found above a limit of 2 mJy. Croft et al. (2010, 2011) presented results from the Allen Telescope Array Twenty-centimeter Survey (ATATS). They surveyed 690 deg^2 of an extragalactic field on 12 epochs. They compared the individual images with their combined image and the combined image with the NRAO VLA Sky Survey (NVSS; Condon et al. 1998). No transients were found above a peak flux density limit of 40 mJy in the combined image, with respect to the NVSS survey (Croft et al. 2010). In addition, no transients were found in the individual epochs above a peak flux density of about 100 mJy (Croft et al. 2011).

A systematic search for transients was made between the two largest radio sky surveys, Faint Images of the Radio Sky at Twenty-Centimeters (FIRST; Becker et al. 1995) and NVSS (Condon et al. 1998) by Levinson et al. (2002). Nine transient candidates were identified. Follow-up observations of these established that only one was a genuine transient—a likely radio supernova in NGC 4216 (Gal-Yam et al. 2006; Ofek et al. 2010). We note that each FIRST and NVSS image is composed of $\approx$4 overlapping beams of adjacent regions taken typically with $\delta t \sim$ days (Becker et al. 1995; Condon et al. 1998; Ofek & Frail 2011). Therefore, if the duration ($t_{\rm dur}$) of the Bower et al. transients is shorter than this typical time between images composing "one epoch" then the sensitivity of these surveys for transients is degraded by $\approx\sqrt{4}$. However, the Levinson et al. survey used a peak flux density limit of 6 mJy, which is ($\gtrsim$2) higher than the flux limit of these surveys. Therefore, its efficiency for Bower et al.-like transients is not degraded.

Bright (>1 Jy), short-lived transients have been reported by the Nasu 1.4 GHz survey (e.g., Matsumura et al. 2009; see Section 1). Croft et al. (2010, 2011) argued that these transients are not real because their implied event rate cannot be reconciled with their own survey unless this population has a sharp cutoff at flux densities below 1 Jy. We note that Croft et al. adopted the Nasu transients areal density reported in Matsumura et al. (2009). However, this areal density is inconsistent with the rate reported in Kida et al. (2008), which is roughly two orders of magnitude lower. Furthermore, based on the Nasu survey parameters reported in Matsumura et al. (2009), we estimate that the areal density of the Nasu transients is roughly two orders of magnitude lower than that stated in their paper. This possible inconsistency was already mentioned by Bower & Saul (2011). However, they adopted the Nasu transients areal density as stated in Matsumura et al. (2009). More information about the Nasu survey is needed in order to resolve this issue.

Here we present an estimate of the rate of transients from the Nasu observations: Matsumura et al. (2009) reported that they discovered (at that time) nine transients over a period of two years (730 days). Assuming that they have four pairs of antennas ($N_{\rm ant}$), each looking at a different position (near the local zenith $\delta \approx 37$ deg) with a field of view of $W = 0.4$ deg and scanning the sky at the sidereal rate, the total sky area scanned by their system after two years is $\approx 3.4 \times 10^5$ deg^2 ($\cong N_{\rm ant} W \times 360 \cos(37^\circ) \times 730$). We further divided this sky area by 1.61 due to the fact that their sensitivity is not uniform within the beam. This correction factor is calculated using Equation (C4) in Appendix C. The total areal density of their transients is the number of transients divided by the total corrected sky area, $\approx 4.3 \times 10^{-5}$ deg^{-2}. Assuming that the transients duration is one day, then their rate is ≈ 0.02 deg^{-2} yr^{-1} ($\approx 4.3 \times 10^{-5}$ deg^{-2} $\times$[365 days yr^{-1}]/[1 day]). We note that our derived Nasu transients rate is roughly consistent with the upper limit on the rate given by Kida et al. (2008). Therefore, we speculate that there was a confusion between areal density and transient rate in the Matsumura et al.'s (2009) paper. We conclude that if our estimate for the areal density for the Nasu transients is correct, then the ATATS survey results cannot decisively rule out the reality of the Nasu transients.

A comprehensive survey at 0.8 GHz was reported by Bannister et al. (2011). They surveyed 2776 deg^2 south of $\delta = -30^\circ$ over a 22 year period. Out of about 30,000 sources they identified 53 variables and 2 transient sources. Recently, Bower & Saul (2011) reported a transient search in the fields of the VLA calibrators in which no transients were found (summarized in Table 1 and Figure 1). Another related work by Bell et al. (2011) searched for radio transients in the fields of the VLA phase calibrators at 1.4 GHz, 4.9 GHz, and 8.5 GHz. Based on their survey parameters (Table 1), we estimate that their 95% confidence surface density upper limit on transients brighter than 8 mJy in 1.4 GHz, 4.9 GHz, and 8.5 GHz are 0.19 deg^{-2}, 0.13 deg^{-2}, and 0.50 deg^{-2}, respectively. These values are corrected for the beam non-uniformity factor (of 1.61) mentioned earlier. We assumed that Bell et al. (2011) searched for transients within the full width at half-power of the beam. For clarity, in Figure 1 we show only the 4.9 GHz limit.

2.2. Surveys at Frequencies above 2 GHz

There have been several additional transient surveys carried out at frequencies above 1.4 GHz. At 3.1 GHz, Bower et al. (2010) report a marginal detection of one possible transient (4.3σ) in a 10 deg^2 survey of the Boötes extragalactic field. In a five-year catalog of radio afterglow observations of 75 γ-ray bursts, Frail et al. (2003) found several strong variables at 5 and 8.5 GHz, but no new transients apart from the radio afterglows themselves.

Two surveys at 5 GHz have specifically targeted the Galactic plane. Taylor & Gregory (1983) and Gregory & Taylor (1986) used the NRAO 91 m telescope to image an approximately 500 deg^2 region from Galactic longitude $l = 40$ deg to $l = 220$ deg with Galactic latitude $|b| \leqslant 2$ deg in 16 epochs over a five-year period. They identified one transient candidate which underwent a 1 Jy flare but for which follow-up VLA observations showed no quiescent radio counterpart (Tsutsumi et al. 1995). They also claimed tentative evidence for a separate Galactic population of strong variables comprising 2% of their sources. Support for this comes from Galactic survey of Becker et al. (2010), who find about one-half of their variable source sample (17/39) or 3% of all radio sources in the Galactic plane, undergo strong variability on 1 year and 15 year baselines. We note that the surface density of radio sources in the Galactic plane is only slightly higher ($\approx$20%) than at high Galactic latitudes (Helfand et al. 2006; Murphy et al. 2007).

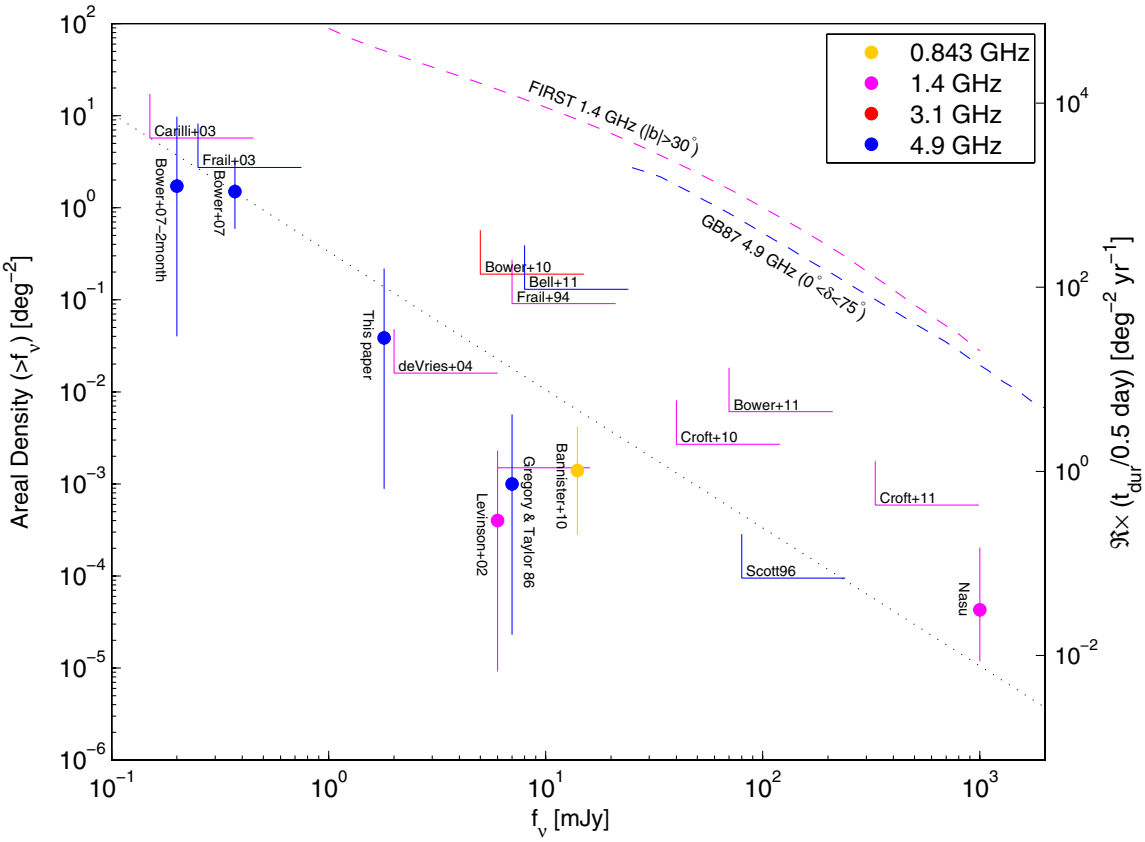

Figure 1. Cumulative areal density of radio sources and transients as a function of peak flux density for various surveys. Different colors represent different frequencies as specified in the legend. 95% confidence upper limits from various transient surveys are shown as right-angle corners, while measured areal densities are marked as filled circles. All the error bars represent 2σ confidence intervals. The dotted line shows an extrapolation of the Bower et al. (2007) transients areal density, assuming that the cumulative source density is proportional to $f^{-3/2}$, where f is the specific flux. The Bower et al. (2007) transients areal density is 1.5 deg^{-2} for sources brighter than 370 μJy. We note that this is a factor of two higher than the areal density used in Ofek et al. (2010). We note that the Nasu survey rate is based on our estimate using the survey description in their papers (see Section 2). Because some of the parameters of this survey are unknown to us, we increase the error bars for this survey to include a factor of two uncertainty. For the Levinson et al. survey, we mark the areal density of the single transient found in this survey (a supernova in NGC 4216). Also marked is the 95% confidence upper limit, shown as an horizontal line near the upper edge of the Levinson et al. error bar, assuming there are no Bower et al. transients in the survey. For the de Vries et al.'s (2004) search, we use a specific flux limit of 2 mJy since they used the FIRST survey in which each epoch is composed of about four observations of the same field taken within $\delta t \approx$ days. Therefore, this degrades their survey sensitivity to Bower et al.'s transients by a factor of about $\sqrt{4}$. The right-hand-side y-axis shows the transients rate assuming a transient duration of 0.5 days. Some surveys are excluded from this plot. For example, Becker et al. (2010) restricted their catalog to sources detected in at least two out of three epochs, or that have a confirmed detection at 1.4 GHz. Therefore, such surveys are not included here. Also shown are the areal densities of persistent sources at 1.4 GHz and 4.9 GHz based on the FIRST and GB87 surveys, respectively (dashed lines).

One of the largest variability surveys of its kind was carried out using the seven-beam receiver on the NRAO 91 m telescope (Scott 1996; Gregory et al. 2001). The sky from $0^\circ \leqslant \delta \leqslant 75^\circ$ was surveyed over two one-month periods in 1986 November and 1987 October (Condon et al. 1989, 1994; Becker et al. 1991; Gregory et al. 1996). The final catalog, made by combining both the 1996 and 1997 epochs, contained 75,162 discrete sources with peak flux densities >18 mJy. Long-term variability information was available for majority of the sources by comparing the mean peak flux densities between the 1986 and 1987 epochs. Scott (1996) carried out a preliminary analysis of the long-term measurements and identified 146 highly variable sources, or $<1\%$ of the cataloged radio sources.

Eight possible transients in the Scott (1996, Table 5.1) list appear in either 1986 or 1987 but are undetected in the other epoch ($<2\sigma$). Two sources are previously identified variables from the Gregory & Taylor (1986) survey, while six are flagged as possible false positives due to confusion by nearby bright sources. One source (B150958.3+103541) was 9 ± 6 mJy in 1986 and 75 ± 7 mJy in 1987 but it is in both the FIRST and NVSS source catalogs. There are therefore no long-term transients identified in the Scott (1996) survey.

In order to estimate the flux density limit above which the Scott (1996) comparison between the 1986 and 1987 surveys is complete, we compared the source numbers near the celestial equator, as a function of specific flux in the two publicly available catalogs from 1987 and the combined 1986/1987 catalog. We found that at flux densities below about 40 mJy, the number of sources, as a function of flux density, in the 1987 catalog is rising slower than that for the one of the deeper combined catalogs. Therefore, we estimate that near the terrestrial equator, the 1987 catalog is complete above a flux density of about 40 mJy. However, these catalogs were made from observations in which each point on the sky was observed $\approx 4/\cos(\delta)$ times taken within a few days. This degrades the sensitivity of the comparison carried out by Scott (1996), for $\lesssim$1 day transients, by about $\sqrt{4}$. Therefore, we conclude that the Scott (1996) survey is sensitive to short-term ($\lesssim$1 day) transients brighter than about 80 mJy ($= 40\sqrt{4}$). Finally, assuming that Scott (1996) did not find any transients in two epochs, we

Table 2
List of Survey Pointings

Field Name	R.A. (deg)	Decl. (deg)	N_{ep}
1851−1327	282.94699	−13.45500	16
1852−1309	283.09963	−13.15668	16
1853−1233	283.40439	−12.56005	16
1853−1251	283.25209	−12.85836	16
1853−1318	283.40625	−13.30508	16

Notes. List of all 141 fields that were observed as part of this survey. The number of epochs per pointing is marked in N_{ep}.

(This table is available in its entirety in a machine-readable form in the online journal. A portion is shown here for guidance regarding its form and content.)

put a 2σ upper limit on the areal density of $\lesssim$1 day transients brighter than 80 mJy, of 9.5×10^{-5} deg^{-2}.

In summary, despite the heterogeneous nature of these GHz surveys, it is clear that the radio sky is relatively quiet compared with the sky in γ-rays. The fraction of strong variables among the persistent radio source population is 0.1%–3% from flux densities of 0.1 mJy to 1 Jy. However, the exact percentage of strong variables is still uncertain because of the different criteria used by various surveys. We note that within this flux density range, radio source populations are dominated by active galactic nuclei (AGNs) roughly above 1 mJy and star-forming galaxies dominate the source counts below 1 mJy (Condon 1984; Windhorst et al. 1985).

The transient areal densities detected by these various surveys, as well as our survey, are shown graphically in Figure 1. Also shown in this figure are the persistent sources areal densities at different frequencies. This plot is further discussed in Section 9.

3. SURVEY OBSERVATIONS

We designed a survey to look for transients and variable sources near the Galactic plane, with typical timescales of days to two years at milli-Jansky flux density levels. We were specially interested in finding transients, conducting multiwavelength follow-up of these events and finding counterparts, and studying their spectral evolution.

3.1. Survey Design

We used the VLA to observe 141 pointings along the Galactic plane. In order to minimize telescope motions, we selected all the pointings in four regions. The median Galactic longitude (l) and latitude (b) of the four regions are $l = 22.6$ deg, $b = -6.7$ deg; $l = 56.6$ deg, $b = -5.5$ deg; $l = 89.7$ deg, $b = -7.8$ deg; $l = 106.0$ deg, $b = -6.5$ deg. Within each region we selected 26–42 pointings within 2.3 deg from the median position of each region. Each pointing was selected to have no NVSS sources brighter than 1 Jy within 3 deg, no NVSS sources brighter than 300 mJy within 1 deg, and no source brighter than 100 mJy within the field of view as defined by the half-power radius. We also rejected fields for which the distance from known Galactic supernova remnants (SNRs; Green 2002) is within twice the diameter of the SNR. The typical distance between pointings in each region is about 20′. The final 141 pointings are listed in Table 2.

3.2. Observations

These 141 fields were observed on 11 epochs using the VLA in 2008 July and August and on five epochs using the Expanded VLA (EVLA) during 2010 July. All observations were made in the compact D configuration, with a maximum baseline of 0.6 km. For the 2008 observations, we added together two adjacent 50 MHz bandwidths centered at 4835 and 4885 MHz with full polarization. For the 2010 observations, we added together two adjacent 128 MHz sub-bands centered at 4896 and 5024 MHz with full polarization.

In 2008, care was taken to ensure that the local sidereal start time was the same for each 3 hr epoch (20:30 LST). Therefore, each field was observed at the same hour angle and subsequently the synthesized beam stayed the same for each epoch, varying only when antennas were taken out of the array. The 2010 observations were taken during EVLA shared-risk science commissioning, and so some scans were lost due to correlator errors and the last two epochs began one hour earlier than our 2008 local sidereal start time.

We integrated each pointing for about 50 s on average. The maximum integration time was 58.5 s and the minimum was 43.3 s. Additionally, during each 3 hr observing run, we carried out all necessary calibrations. Amplitude calibration was achieved with observations of 3C 286 and 3C 147 at the start and end of each epoch, respectively. Phase calibration was checked every 20–25 minutes by switching to a bright point source within a few degrees of the targeted region. We used the following four phase calibrators (one per region): J1911−201, J1925+211, J2202+422, and J2343+538. The total calibration and antenna move-time overhead was about 30% of the observing time. This overhead on move time could have been lowered had we used the fast slew methods from the NVSS and FIRST surveys (Condon et al. 1998; Becker et al. 1995), with a resulting increase in the number of square degrees of sky surveyed per hour. However, since we recently found that this method could introduce spurious transients (Ofek et al. 2010), we adopted a less efficient but more robust observing method.

In Table 3, we list the time of the UTC midpoint for each epoch with some additional information. The shortest variability timescale sampled was 24 hr and the longest was $\cong$2 yr. By design, the cadence of the 2008 survey was chosen to probe variability timescales between a day and a month. A longer 2 yr timescale was also sampled by comparing deep images made from the 2008 and 2010 campaigns (see below).

4. DATA REDUCTION AND CALIBRATION

In 2008, the uv data were streamed directly to a disk in real time, and a pipeline was run after each of the four regions was observed. We used the data reduction pipeline provided in the Astronomical Image Processing System (AIPS) package.[9] For each epoch, the pipeline first flagged and calibrated the uv data. It then imaged a 30 arcmin wide field around all 141 pointings, deconvolving down to three times the rms noise and restoring the image with a robust weighted beam. No self-calibration was done. The VLA data rates ($\approx$30 Mbytes hr^{-1}) and the D-configuration image requirements (512 pixels, 3.″6 pixel^{-1}) were so modest that the entire pipeline reduction and the variable source analysis (see Section 5) was completed before the VLA finished observing the next region ($\approx$40 minutes). The real-time

[9] http://www.aips.nrao.edu/

Table 3
Observing Epochs

Epoch	Date (UTC)	Time Elapsed (days)	⟨rms Noise⟩ (μJy)	Observed Fields	Number of Sources	Gain Correction	Cosmic Error (%)
1	2008 Jul 15.40	0.00	243	141	343	1.029	5.3
2	2008 Jul 18.39	2.99	181	141	155	0.987	4.6
3	2008 Jul 19.39	3.99	229	141	363	1.033	4.6
4	2008 Aug 10.33	25.93	178	141	166	0.971	1.0
5	2008 Aug 11.33	26.93	183	141	164	0.980	1.1
6	2008 Aug 14.32	29.92	174	141	162	1.002	0.4
7	2008 Aug 16.31	31.91	173	139	151	1.023	1.7
8	2008 Aug 18.29	33.89	178	141	155	0.924	1.7
9	2008 Aug 25.29	40.89	196	141	183	1.016	2.4
10	2008 Aug 28.28	43.88	178	141	157	0.956	3.5
11	2008 Aug 30.28	45.88	186	141	170	1.033	5.3
12	2010 Jul 16.42	731.02	105	141	216	1.020	1.9
13	2010 Jul 18.43	733.03	111	134	199	1.022	0.8
14	2010 Jul 22.35	736.95	108	109	158	0.992	0.6
15	2010 Jul 23.32	737.92	104	141	200	1.008	0.7
16	2010 Jul 25.31	739.91	116	140	217	1.003	2.1

Notes. List of the 16 epochs. The dates indicate the observations mid-time. In practice, in all the instances in which we find that the cosmic error is smaller than 3% we replaced it by 3% (see Section 6). The numbers of sources detected in each epoch are fluctuating due to the fact that we used a uniform flux density threshold for all epochs (see Section 4).

Table 4
Survey Parameters

Property	Value
Frequency	4.9 GHz
Observing time	48 hr
Survey area	2.66 deg^2
Angular resolution	15″
Repeats	16
Timescales	1 day–2 years
Number of fields	141
Mean exposure time per field	50 s
Mean rms per epoch (2008)	190 μJy
Mean rms per epoch (2010)	109 μJy
Mean rms per 11 epochs (2008)	72 μJy
Mean rms per 5 epochs (2010)	56 μJy
Mean rms in Master images	46.7 μJy

analysis capability was not available in 2010 but the data were also calibrated within AIPS following standard practice.

As the experiment progressed we built up reference images, made by summing all previous epochs. These deeper images proved useful in the real-time search for transient sources (Section 5). After the survey was completed, a final set of images was made separately for each yearly campaign using the data from the 11 epochs in 2008 and the five epochs in 2010. We also summed the 2008 and 2010 deep images to create 16-epoch Master images for the entire experiment. In summary, there were three final image data sets; the Single epoch images, the Yearly images (for 2008 and 2010 separately), and the final Master images made from all available data.

Our final survey parameters are given in Table 4. The effective survey area was calculated using the full width at half-power (9.′3 at 4.86 GHz) but the searches for transients in real-time and for variability were made over a larger area—out to the 15% response point of the primary beam (15′ diameter). For the analysis, no correction was made for the primary beam attenuation, in order to maintain uniform noise statistics over the entire field. The synthesized beam and rms noise estimates for different epochs and different pointings varied by factors close to unity. The values in Table 3 are averages for each epoch over all pointings, while Table 4 gives the mean rms values (over all fields) in the Master images and the 2008 and 2010 combined images.

Throughout the paper, we state explicitly if we use corrected or uncorrected flux densities. "Corrected flux densities" are corrected for beam attenuation and for the CLEAN bias by adding additional +0.3 mJy (e.g., Becker et al. 1995; Condon et al. 1998). In order to maintain uniform statistics, we chose to search all images to the same depth, rather than compute a new threshold for each image individually. In practice, this led to some false positives for noisier than average epochs and fields with bright point sources. Indeed, Table 3 indicates that the noisiest epochs contain larger number of sources.

5. REAL-TIME TRANSIENT SEARCH

We employed two distinct analysis strategies for transient and variable source identification. The first, which is discussed in this section, was a real-time analysis. The main motivation was to rapidly identify any short-lived sources and mark them for immediate follow-up at other wavelengths. The second was a post-survey analysis which was carried out after all the epochs had been observed. The main goals of this second phase were to carry out a more in-depth search for transients (Section 6) and to characterize the variability properties of the persistent source population (Section 7).

For the real-time identification, the images (Section 4) were searched visually for any new or strongly varying sources by comparing them with individual epochs, and by comparing them with a reference image made by summing all previous epochs. Any candidate variable source which we identified was subject to a more detailed light curve and position-fitting analysis before deciding to trigger radio, optical, and/or X-ray follow-up observations.

The follow-up visible light observations were carried out using the robotic Palomar 60″ telescope (P60; Cenko et al. 2006) and the Keck-I 10 m telescope. The UV and X-ray observations

Table 5
Single Epoch Catalog

Epoch	Source	Field Name	J2000 R.A. (deg)	J2000 decl. (deg)	$f_{\nu,p}^{\rm cor}$ (mJy)	$f_{\nu,p}^{\rm uncor}$ (mJy)	σ_p (mJy)	f/f_p	Major ($''$)	Minor ($''$)	P.A. (deg)	Δ_C ($'$)
1	1	1851–1327	282.955970	−13.502335	33.49	25.39	0.26	1.03	23.67	13.67	23.7	2.89
1	2	1851–1327	282.937502	−13.432227	1.62	1.23	0.26	1.00	23.49	13.31	29.7	1.48
1	3	1851–1327	282.855004	−13.349517	10.53	1.12	0.26	0.64	23.66	8.48	13.6	8.30
1	4	1853–1233	283.399554	−12.561197	6.90	6.59	0.26	0.95	21.88	13.15	20.3	0.29
1	5	1853–1233	283.474902	−12.562245	5.67	3.10	0.26	0.89	22.97	11.74	21.5	4.13

Notes. Catalog of 2953 sources detected in Single epochs. Column descriptions: epoch is the epoch number (see Table 3), and source is a serial source index in epoch. $f_{\nu,p}^{\rm cor}$, $f_{\nu,p}^{\rm uncor}$, and σ_p are the corrected peak flux density, uncorrected peak flux density, and the error in the uncorrected peak flux density, respectively. Corrected fluxes are corrected for beam attenuation and the CLEAN bias. f/f_p is the integrated flux density divided by the peak flux density. Major and Minor are the major and minor axes of the object size, while P.A. is the position angle of the major axis. Finally, Δ_C is the distance of the source from the beam center.

(This table is available in its entirety in a machine-readable form in the online journal. A portion is shown here for guidance regarding its form and content.)

were conducted by the *Swift* satellite (Gehrels et al. 2004). We note that prior to and during the VLA campaign we obtained visible light reference images for most of our fields using the P60 telescope.

We identified two possible transients that were deemed interesting enough for multiwavelength follow-up. However, follow-up VLA observations and a careful post-observing reanalysis (Section 7) showed that these are not real transients. One source, J213438.01+414836.0, was a sidelobe artifact, while the second source, J230424.68+530414.7, is a long-term variable that had crossed our single-epoch noise threshold on 2008 July 19 (which was a noisy epoch) and is clearly seen in the 2008 and 2010 deep co-adds. We note that both sources were observed using the P60 telescope about 2 hr and 1 hr after the radio observations were obtained, respectively. Furthermore, *Swift* X-Ray Telescope (XRT) observations of the first source were obtained about five days after it was found. These fast response observations demonstrate our near real-time follow-up capabilities.

6. POST-SURVEY SOURCE CATALOG

The next phase of our analysis occurred after the conclusion of the observations. We generated source catalogs in order to search for short-lived transients and to carry out a variability study of all identified sources. The AIPS task SAD (search and destroy) was used for source finding.

We found that false positive sources came from one of two main reasons: slightly resolved sources and sidelobe contamination. Point sources were identified by requiring that their integrated flux density was within a factor of two of their peak flux density. False sources created by scattered power from the snapshot sidelobe response was only a significant problem for the six fields with sources whose peak flux density exceeded 20 mJy. We flagged any variables or transients from these fields for visual inspection.

Three catalogs were created. The first catalog is the "Single epoch catalog," generated by running *SAD* on a 15 arcmin diameter region for each single-epoch image individually (Table 5). A second "Master catalog" (Table 6) was created by running SAD on the final Master images made from all available data (16 epochs), while a third catalog, "Yearly catalog," was generated on the yearly images (for 2008 and 2010 separately).

The Master catalog has the advantage of being able to identify persistent radio sources approximately $\sqrt{N}$-times fainter than any individual epoch (where $N = 16$), but it is $\sqrt{N}$-times less sensitive to a short-lived transient that might be identified in a single-epoch image. For our Single epoch catalogs, we used a peak flux density cutoff of 1 mJy in 2008 and 0.76 mJy in 2010, and the number of sources in each epoch is given in Table 3. Our Master catalog consisted of 464 sources which are listed in Table 6, with a peak flux density cutoff of 0.28 mJy. The Yearly catalog had a peak flux density cutoff of 0.5 mJy in 2008 and 0.35 mJy in 2010. These cutoffs correspond to about a 5σ–7σ threshold, depending on the rms noise for individual fields. The online version of the Master catalog also contains the peak-specific flux of each source in all the epochs. This was measured in the Single epoch images at the position of the sources found in the Master image.

We used the Master catalog to perform a second-order amplitude calibration that would tie together the flux density scale for all epochs. Normally, self-calibration could be used to find additional gain variations within a radio observation but our survey was designed to avoid pointings with bright point sources. Our approach assumes that each VLA epoch (all the observations in each epoch were taken within 3 hr) shares the same "gain" correction, and we solved for these "nightly" gain corrections by fitting, using least-squares minimization, the equation

$$m_{ij} = z_i + \bar{m}_j, \quad (1)$$

where m_{ij} is the "magnitude": $-2.5\log_{10} f_{ij}$, f_{ij} is the peak-specific flux of the jth source in the ith epoch, z_i is the gain correction for the ith epoch (in units of magnitudes), and $\bar{m}_j$ is a nuisance parameter representing the best-fit mean magnitude of the jth source. We note that, as explained in Appendix A, magnitudes have convenient statistical properties. The final multiplicative gain corrections are $10^{-0.4 z_i}$. This method is described in detail in Appendix A, and the best-fit multiplicative gain corrections are listed in Table 3. Similarly, we also derived the yearly gain corrections for the Yearly epochs. These gain corrections are 1.004 and 0.996 for 2008 and 2010, respectively.

The flux density errors reported by SAD do not include any systematic error terms. Typically, VLA calibration is assumed to be good to a level of 3% or better (e.g., Condon et al. 1998). In order to check if some epochs are noisier, we estimated the "cosmic errors," $\epsilon_{\rm cos}$, using the following scheme. We measured the standard deviation in the specific flux of the four phase calibrators observed on each night, after normalizing their flux density by their mean-specific flux over all the epochs taken at the same year. The cosmic errors estimated using this method are listed for each epoch in Table 3. This estimate is based on a small number of sources and these sources may be variable. Therefore, this should be regarded as a rough estimate. In some

Table 6
Master Catalog

		Current Search									NVSS		USNO	2MASS
J2000 R.A. (deg)	J2000 decl. (deg)	$f_p^{\rm cor}$ (mJy)	$f_p^{\rm uncor}$ (mJy)	σ_p (mJy)	$N_{\rm obs}$	$N_{\rm det}$	χ^2	StD/$\langle f \rangle$	χ^2_Y	StD/$\langle f \rangle_Y$	Dist ($''$)	$\alpha^{\rm a}$	Dist ($''$)	Dist ($''$)
283.675661	−13.518385	7.24	2.48	0.05	15	15	50.23	0.17	2.54	0.06	1.0	1.03	...	...
283.682476	−13.444363	2.52	1.85	0.05	15	15	52.34	0.18	0.05	0.02	3.8	0.17	...	...
284.193460	−13.325061	47.83	32.01	0.10	14	14	70.30	0.08	0.48	0.02	0.9	−0.07	...	0.6
284.387195	−12.213881	11.03	6.74	0.06	15	15	142.60	0.14	2.85	0.05	4.4	−0.54	...	...
283.976980	−12.165968	93.19	57.18	0.13	15	15	468.40	0.18	68.27	0.25	0.9	0.08	...	...
283.949467	−11.356239	7.65	4.69	0.05	15	14	53.20	0.10	0.84	0.03	2.9	1.14	...	...
284.592955	−10.949209	13.07	10.66	0.06	15	15	48.94	0.08	3.98	0.06	4.2	1.26	...	...
284.497521	−10.459850	2.70	2.11	0.05	15	14	46.02	0.14	1.71	0.06	10.0	0.83	...	...
298.720898	16.755257	10.92	8.39	0.04	16	16	118.76	0.10	5.02	0.08	1.0	−0.80	...	...
299.583716	18.171732	6.93	5.82	0.04	16	16	143.31	0.14	15.03	0.12	2.3	−0.20	...	...
299.271523	18.226378	4.81	3.65	0.05	16	16	75.27	0.12	0.67	0.04	...	...	...	...
299.353219	18.473931	41.09	6.89	0.05	16	16	149.27	0.13	13.66	0.13	0.4	0.14	...	...
300.337088	19.936532	7.71	5.50	0.04	16	16	55.62	0.08	0.12	0.01	2.2	0.49	...	...
300.030673	20.034572	23.81	4.23	0.04	16	16	70.42	0.11	0.69	0.02	0.6	0.39	...	...
324.719526	42.022609	4.34	3.83	0.05	16	16	154.53	0.16	20.39	0.17	...	...	...	...
325.523312	42.023491	12.85	2.83	0.04	16	16	356.39	0.20	30.28	0.20	1.0	0.88	...	...
325.348791	42.085546	7.61	2.23	0.04	16	16	148.57	0.15	8.95	0.12	0.3	1.42	...	...
326.519678	42.141397	30.49	8.09	0.04	16	16	54.95	0.06	2.98	0.05	0.5	1.09	...	...
325.966278	42.884463	7.55	2.34	0.05	16	16	46.73	0.15	0.45	0.02	...	...	...	...
326.391328	43.460876	7.24	4.02	0.04	16	16	46.97	0.10	0.32	0.01	1.8	1.00	...	...
341.141889	51.541980	15.60	12.43	0.05	16	16	160.78	0.10	0.53	0.03	1.6	0.54	0.3	...
342.654997	52.100799	24.51	13.77	0.05	16	16	195.40	0.11	18.74	0.13	1.8	0.28	0.6	0.5
341.820302	52.137525	4.11	2.64	0.04	16	16	49.55	0.12	0.43	0.03	1.9	0.66	0.4	1.1
343.612547	52.339910	9.04	7.77	0.05	16	16	168.64	0.12	8.37	0.10	1.2	−0.38	...	...
344.074222	52.431561	4.50	2.92	0.04	16	16	353.19	0.28	35.95	0.24	...	...	1.5	...
342.837121	52.495055	3.85	3.53	0.04	16	16	102.16	0.16	4.92	0.07	5.6	0.39	...	...
346.017848	52.735617	10.19	2.48	0.04	16	16	181.08	0.22	5.30	0.10	4.3	−1.12	...	...
345.504754	52.912710	2.13	1.69	0.04	16	14	91.42	0.25	1.59	0.06	...	...	...	...
345.245407	53.186497	33.34	24.81	0.05	16	16	46.53	0.06	0.86	0.02	0.8	0.91	...	...
346.421593	53.202481	8.26	3.30	0.05	16	16	71.60	0.15	0.18	0.01	6.4	0.35	0.1	...
283.976980	−12.165968	93.19	57.18	0.13	15	15	468.40	0.18	68.27	0.25	0.9	0.08	...	...
298.658519	18.200598	3.28	0.38	0.04	16	0	41.38	0.55	18.72	0.68	...	...	0.8	0.3
299.358645	18.324890	3.02	0.87	0.05	16	5	26.51	0.22	23.36	0.37	2.0	1.03	...	...
299.811372	18.369894	1.82	0.94	0.04	16	6	62.65	0.29	22.02	0.34	...	...	...	...
323.729857	41.317576	0.91	0.55	0.05	16	0	28.52	0.34	20.48	0.53	...	...	1.6	2.0
324.109846	41.657383	1.55	0.45	0.05	16	0	70.45	0.64	23.78	0.67	...	...	...	...
324.719526	42.022609	4.34	3.83	0.05	16	16	154.53	0.16	20.39	0.17	...	...	...	...
325.523312	42.023491	12.85	2.83	0.04	16	16	356.39	0.20	30.28	0.20	1.0	0.88	...	...
342.654997	52.100799	24.51	13.77	0.05	16	16	195.40	0.11	18.74	0.13	1.8	0.28	0.6	0.5
344.074222	52.431561	4.50	2.92	0.04	16	16	353.19	0.28	35.95	0.24	...	...	1.5	...

Notes. A catalog of the 464 sources detected in the Master images. We note that SAD detected additional sources which are not listed here. These sources were identified as noise artifacts by subsequent inspection of the images and were removed from the catalog. Column descriptions: $f_{\nu,p}^{\rm cor}$, $f_{\nu,p}^{\rm uncor}$, and σ_p are described in Table 5. $N_{\rm obs}$ is the number of epochs in which the source position was observed, while $N_{\rm det}$ is the number of detections in the Single epoch images. Subscript "Y" in χ^2 and StD/$\langle f \rangle$ indicates that these values are calculated for the Yearly epochs. Dist is the distance between the radio position and the NVSS, USNO-B1, and Two-Micron All-Sky Survey (2MASS; Skrutskie et al. 2006) nearest counterparts. A portion of the full table containing the 30 Single epoch variable sources (Section 8.1) and the 10 Yearly variable sources (Section 8.2) is shown here for guidance regarding its form and content. The two variable lists are separated by horizontal line. The online table also contains additional columns as the field name, sidelobes flag, integrated flux density divided by peak-specific flux, major axis, minor axis, and position angle of the sources, distance from the beam center, V_R and V_F for the yearly specific fluxes, the NVSS flux density, the B and R magnitudes of the USNO-B counterparts, J, H, and K-magnitudes of the 2MASS counterparts, and all the 16 peak flux densities and error measurements in the Single epochs and the peak flux density measurements in the Yearly images. We note that the distance threshold for the USNO-B and the 2MASS counterparts was set to $2''$, and $15''$ for the NVSS.

[a] The spectral power-law slope, defined by $f_\nu \propto \nu^\alpha$, as measured from the NVSS 1.4 GHz specific flux and our 4.9 GHz corrected flux density.

(This table is available in its entirety in a machine-readable form in the online journal. A portion is shown here for guidance regarding its form and content.)

instances, the cosmic errors we estimated were smaller than 3% and in those cases we replaced the cosmic errors for these epochs by 3%. We note that if indeed the cosmic errors in some cases are smaller than 3%, then our strategy of adopting a larger cosmic error may reduce the number of variables found in our survey. For the Yearly catalogs, we used the mean cosmic error terms of the individual epochs in each year. These are 0.028 and 0.012 for 2008 and 2010, respectively.

Equipped with the gain corrections and an estimate for the cosmic errors, we next corrected the flux density measurements of all the sources using the gain correction factors and added in quadrature the cosmic errors to the peak flux density errors. The

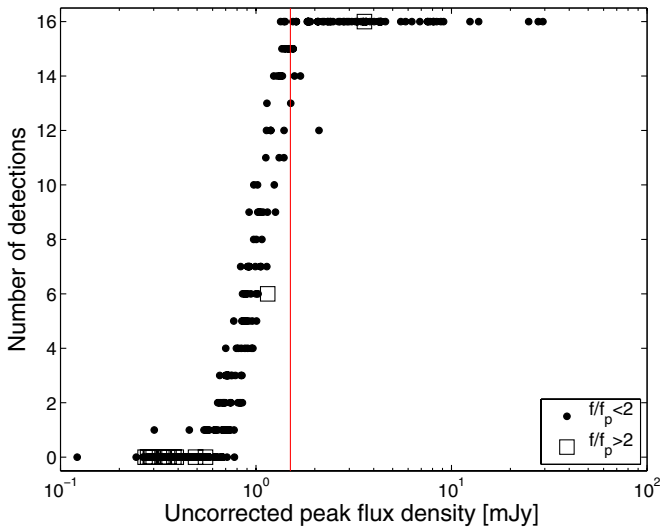

Figure 2. Detection repeatability as a function of flux density. For each source whose field was observed 16 times and which was detected in the Master catalog, the plot shows the number of SAD detections in individual epochs as a function of the peak flux density. The number of detections is shown against the uncorrected peak flux density of the source as measured in the Master image. Point sources are represented by filled circles, while open squares are for resolved sources. The vertical line shows the 1.5 mJy cut we used to define our completeness limit.

(A color version of this figure is available in the online journal.)

new specific fluxes and errors were used in all the plots and the calculation of the statistical properties of the light curves.

7. POST-SURVEY TRANSIENT SEARCH

Our final transients search utilized the catalogs presented in Section 6. Specifically, we matched all the sources in the individual epochs to sources in the Master catalog using a 4″ matching radius. Sources in individual epochs which do not have a counterpart in the Master catalog are transient candidates. However, because we used a single flux density threshold, while the noise varies in each epoch and field, most of the faint sources are probably noise artifacts. We used Figure 2 in order to choose a reasonable flux density limit for our transient search. This figure shows the number of detections, in the Single epoch catalogs, of sources which were detected in the Master catalog and had their field observed 16 times. This plot suggests that the probability that a faint source detected in the Master image will be detected with uncorrected flux density above 1.5 mJy, in only one epoch, is low. In fact, it suggests that we could use a threshold even lower than 1.5 mJy. However, given that this is based on small number statistics and given the variable quality of different images, we used a higher specific flux limit cutoff of 1.5 mJy.

Following this analysis, we searched for sources detected in a single epoch that do not have a counterpart in the Master catalog, have uncorrected flux density >1.5 mJy (6σ–14σ), and a distance from beam center smaller than 4.′65 (i.e., half-power beam radius). In total, we found 50 sources. However, a close inspection of these sources shows that most of them are not real. Of the 50 candidates, 46 are in fields which contain sources brighter than 10 mJy, and they are clearly the results of sidelobes. Of the remaining four candidates, three sources are also most probably not real. One candidate was found next to a slightly resolved 5 mJy source. A second object is a known 2 mJy source for which the centroid position shifted by a quarter of a beam in one of the epochs, a third candidate is a sidelobe seen in several epochs, and the fourth candidate is probably a real transient. This transient candidate, J213622.04+415920.3, is described next.

Table 7
Properties of the Transient Candidate J213622.04+415920.3

Property	Value
Field name	2136+4158
R.A. (J2000.0)	$21^{h}36^{m}22^{s}.04 \pm 1''.2$
Decl. (J2000.0)	$+41°59'20''.3 \pm 1''.2$
Detection date	2008 Jul 15.4147
Uncorrected peak flux density	1.61 ± 0.28 mJy
Corrected peak flux density	2.36 ± 0.41 mJy
Distance from beam center	2.′77

Notes. We note that the coordinates in this table are based on Gaussian fit. The coordinates of this source in the Single epoch table (Table 5) were derived using SAD and they are somewhat different R.A. $= 21^{h}36^{m}21^{s}.965$, decl. $= +41°59'21''.52$ (J2000.0). Note that the flux density is corrected also for the CLEAN bias.

7.1. The Transient Candidate J213622.04 + 415920.3

We found a single source, J213622.04 + 415920.3, that was detected only in the first epoch and may be a real transient. Given that this source was detected in the first epoch, before we constructed a reference image, it was not followed up in real-time. The main properties of this transient candidate are summarized in Table 7. The peak flux density measurements at the position of the source at all epochs show that the source was indeed visible only in the first epoch. Moreover, this source is not detected in the Master or Yearly images. The peak-specific flux at this position in the Master image is 74 ± 42 μJy, and in the 2008 (2010) combined images is 161 ± 67 μJy (-14 ± 49 μJy).

In order to test if the source is variable during the 46 s VLA integration, we split the data into two 23 s images. We found that the flux density of the source did not change significantly between the first and second parts of the exposure. This transient was found in the first epoch of our survey and, therefore, we cannot put any upper limit on its duration.

The field of J213622.04 + 415920.3 was observed with the P60 telescope in the i band about two days after the transient was detected.[10] This image is shown in Figure 3. We find two sources near the transient position. One source is found $\cong 3''.2$ northeast of the transient location and has an i-band magnitude of 20.98 ± 0.23. The other is found $\cong 2''.3$ south of the transient position and has a magnitude of 19.46 ± 0.20. The magnitudes are calibrated relative to USNO-B1.0 I-band magnitude (Monet et al. 2003). Given the relatively large angular distances between the transient position and the nearest visible light sources, they are probably not associated. We note that given the stellar density in this region the probability of finding a source within a 2.″4 radius from a random position is about 15%.

On 2011 April 28 and May 2 we observed the field of J213622.04+415920 using *Swift*/XRT with a total integration time of 6099 s. We place an upper limit of 0.0012 counts s^{-1} (95% confidence), in the 0.2–10 keV band, on the source counts rate. Finally, we do not find any counterpart to this transient in the SIMBAD, NED, or HEASARC databases.

The search method described in the beginning of this section may miss transients which are bright enough to be present in the

[10] The P60 observations were taken without knowing about the transient, as part of a program to get visible light images of our VLA survey footprints.

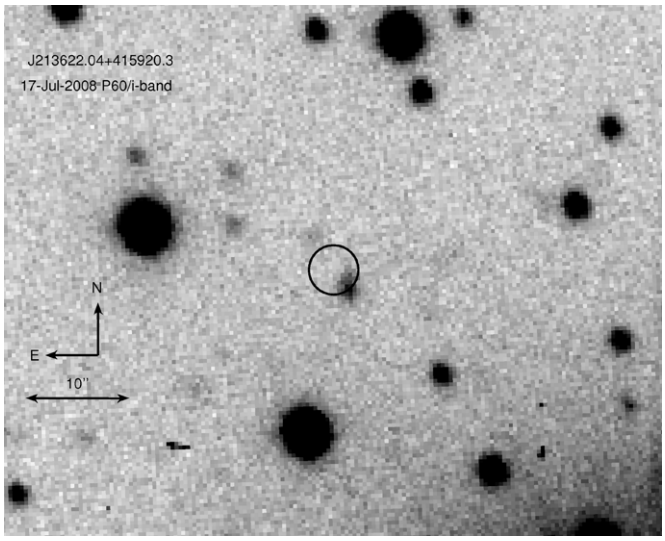

Figure 3. P60 *i*-band image of the field of J213622.04 + 415920.3. The image, with exposure time of 540 s, was taken on 2008 July 17.45. A 2.″4 radius circle marks the transient candidate location. This radius roughly corresponds to the 2σ error circle.

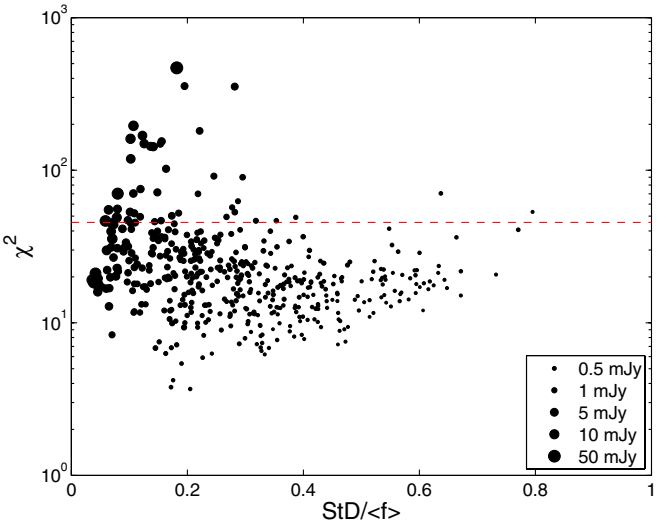

Figure 4. StD/$\langle f \rangle$ vs. χ^2, where the uncorrected peak flux density of the sources (in the Master catalog) is marked by symbol size. The dashed line corresponds to $\chi^2 > 45.5$, which corresponds to 4σ assuming 15 dof.

(A color version of this figure is available in the online journal.)

Master catalog. Therefore, we also searched for sources which are detected in the Master catalog and detected in only one of the Single epoch catalogs with uncorrected flux density above 1.5 mJy. No such sources were found.

8. VARIABILITY ANALYSIS

We investigated the variability of all the sources in the Master catalog using their peak flux densities measured in the Single epoch images (Section 8.1) and the Yearly images (Section 8.2). We used various statistics to assess the variability and its significance, which we list in Table 6. For each source, we calculated its standard deviation (StD) over all the flux density measurements, the StD over the mean flux density (StD/$\langle f \rangle$), and χ^2, given by

$$\chi^2 = \sum_i^N \frac{(f_i - \langle f \rangle)^2}{\sigma_i^2 + (f_i \epsilon_{\cos,i})^2}, \quad (2)$$

where N is the number of measurements and which is 2 for the Yearly catalogs and 16 for the Single epoch catalogs, i is the epoch index, f_i is the gain corrected peak flux density in the ith epoch, σ_i is its associated error, $\epsilon_{\cos}$ is the cosmic error, and $\langle f \rangle$ is the mean-specific flux of the source over all the epochs. Note that in Table 6, χ^2 is measured over the individual epochs, while χ^2_Y is measured over the two yearly epochs. In the first case, the number of degrees of freedom (dof) is 15, while in the second case it is one.

Some previous surveys have defined "strong variables" as exceeding some pre-defined variability measure. There are many definitions of fractional variability in the literature and for comparison with other surveys we list in the online version of Table 6 the two following indicators:

$$V_R = \frac{\max\{f_i\}}{\min\{f_i\}} \quad (3)$$

and

$$V_F = \frac{\max\{f_i\} - \min\{f_i\}}{\max\{f_i\} + \min\{f_i\}}. \quad (4)$$

We note that these two quantities are related through $V_F = (V_R - 1)/(V_R + 1)$. However, as neither of these indicators accounts for measurement errors, they cannot be used reliably on their own at low flux densities where the measurement errors are very large. Most importantly, estimators involving the min or max functions strongly depend on the number of measurements. This fact complicates direct comparison between different surveys. For example, a light curve whose flux densities are drawn from a log normal random distribution, with $N_{\rm ep} = 3$ survey, and StD/$\langle f \rangle = 0.5$ has $\langle V_R \rangle \cong 2.44$, while for $N_{\rm ep} = 16$ it will have $\langle V_R \rangle \cong 5.62$. Therefore, although Becker et al. (2010) and Taylor & Gregory (1983) defined strong variables identically, i.e., $V_R \geqslant 3$ ($V_F \geqslant 0.5$), any direct comparison of these two surveys is difficult since the number of epochs in these surveys were 3 and 16, respectively. In the future, in order to cope with this problem we suggest the use of StD/$\langle f \rangle$ as a fractional variability estimator. Moreover, in Appendix B we provide a conversion table for V_R as a function of $N_{\rm ep}$ and StD/$\langle f \rangle$.

8.1. Short Timescale Variability

In order to explore radio variability on short timescales (e.g., days to weeks), we constructed 16 epoch light curves for all sources with a mean peak flux density larger than 1.5 mJy ($\approx 6\sigma$). Figure 4 shows the StD/$\langle f \rangle$ versus χ^2 of all sources in the Master catalog. This figure suggests that a large fraction of at least the bright radio sources with flux densities larger than about 10 mJy are variables at the level of $\gtrsim$5%.

In total, we find that 30% (30 out of 98) of the sources in our survey, which are brighter than 1.5 mJy, are variables (at the 4σ level[11]). The light curves of these 30 variable sources are presented in Figure 5, and their flux density measurements and basic properties are listed in Table 6. This is considerably larger than the fraction of variables reported in some of the other "blind" surveys listed in Table 1 (e.g., Gregory & Taylor 1986; de Vries et al. 2004; Becker et al. 2010). A possible explanation

[11] Assuming Gaussian noise, 4σ corresponds to a probability of $\cong 1/15{,}000$ while the number of measurements in our experiment (number of epochs multiplied by the number of sources) is $\approx$7400.

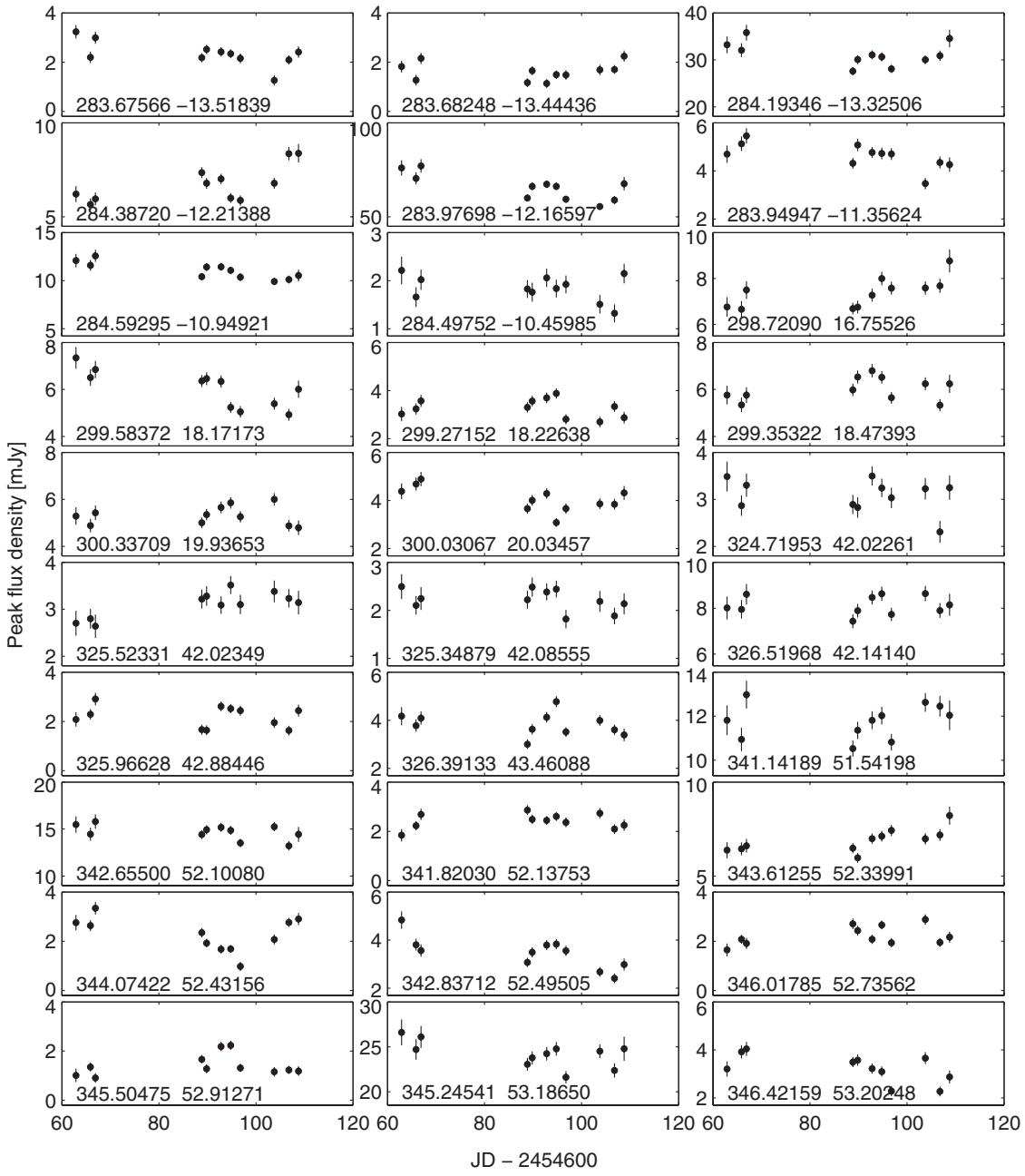

Figure 5. Light curves of the 30 variables which have $\chi^2 > 45.5$. For scaling purposes, we show only the 11 observations taken during 2008. In each panel, we give the J2000.0 right ascension and declination of the source (deg). The individual flux density measurements are given in the online version of Table 6.

for this apparent discrepancy is that the sources in these surveys were extracted from mosaic images in which each point in the survey footprint was observed multiple times during several days. Therefore, the specific fluxes they reported are averaged over timescales of several days (column δt in Table 1). Such measurements will tend to average out variability on timescales which are shorter than δt. In order to test this hypothesis, we carried out a structure function analysis.

We calculated the mean discrete autocorrelation function, $C(\tau)$, of all the 30 variable sources, as a function of the time lag τ. We first normalized each source light curve by subtracting its mean and then dividing it by its (original) mean. We treated all these light curves as a single light curve by concatenating them with 2000 days gaps in between light curves. These gaps are larger than the time span of the individual light curves. We then followed the prescription of Edelson & Krolik (1988) for calculating the discrete autocorrelation function. The errors were calculated using a bootstrap technique with 100 realizations for the measurements in each time lag (e.g., Efron 1982; Efron & Tibshirani 1993). The mean autocorrelation function is presented in Figure 6 (black circles). The autocorrelation at lag "zero" is not one. This is because at lag zero we used a lag window of 0 to +2 days. Therefore, it does not contain only zero lag data. The autocorrelation function reaches zero correlation at $\tau \approx 10$ days.

Next, we calculated the structure function, SF(τ), of these light curves defined by

$$\mathrm{SF}(\tau) = \sqrt{2S^2(1 - C[\tau])} \pm \frac{2S^2 \Delta C[\tau]}{2\sqrt{2S^2(1 - C[\tau])}}, \qquad (5)$$

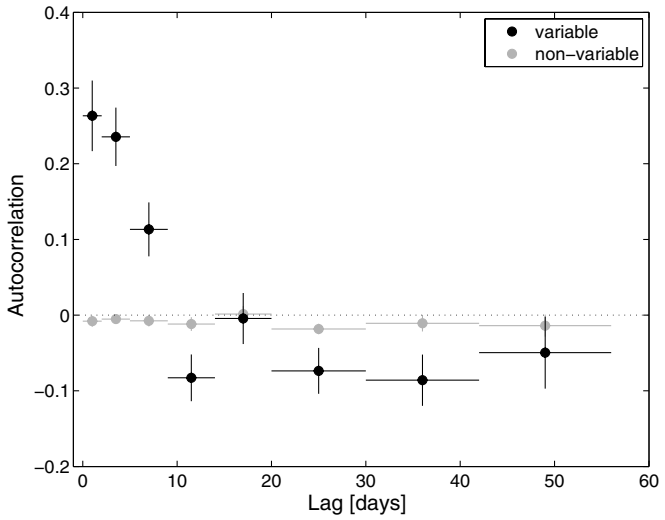

Figure 6. Mean discrete autocorrelation function of all the 30 variable sources (black circles). The gray circles show the same but for all the non-variable sources (see the text). Each light curve was normalized by subtracting its mean and dividing it by its mean. The vertical error bars represent the 1σ errors calculated using the bootstrap method. The horizontal "error bars" represent the full width of the lags contained within each bin. The horizontal dotted line marks zero correlation.

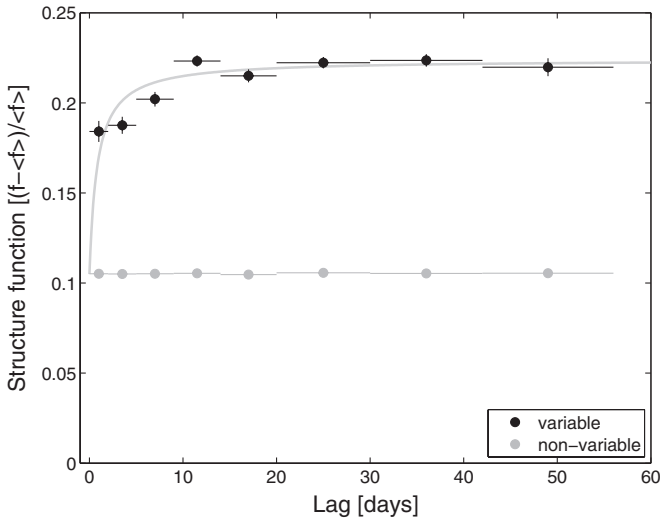

Figure 7. Mean structure function of the normalized light curves as a function of lag, τ. Symbols as in Figure 6. Following Lovell et al. (2008), we fit the structure function (after subtracting the non-variable sources structure function) with the function $m_s\tau/(\tau + \tau_{char})$. The heavy gray line represents the best-fit function, and the best-fit parameters are $m_s = 0.119 \pm 0.003$ and $\tau_{char} = 0.83^{+0.27}_{-0.23}$ days (χ^2/dof = 26.6/6).

where S is the standard deviation of the normalized light curves and $\Delta C[\tau]$ is the bootstrap error in the discrete autocorrelation function. The second term on the right-hand side of Equation (5) represents the error in the structure function. The structure function is presented in Figure 7. Also shown in Figures 6 and 7 are the autocorrelation and structure functions, respectively, for "non-variable" sources (gray symbols) calculated in the same way as for the variable sources. In this context, our selection criteria for non-variable sources are specific flux larger than 2 mJy and $\chi^2 < 25.3$. This χ^2 value corresponds to 2σ confidence, assuming 15 dof.

The structure function of the variable sources, after subtracting the non-variable source structure function, rises rapidly from zero to ≈0.05 on a timescale of the order of one day and then rises to a level of ≈0.12 at lags of ≈10 days at which it stays roughly constant. However, we cannot rule out that it is slowly rising on $\tau > 10$ days timescales.

This analysis suggests that a large component of the variability happens on timescales shorter than about one day. A plausible explanation is that the short timescale variability is due to refractive scintillations and it is discussed in Section 9.2 (e.g., Rickett 1990). This level of variability was likely missed by some previous surveys (Table 1) due either to their choice of frequency (ν), cadence (N_{ep}), or the observing time span (δt). On the other hand, 5 GHz surveys of flat-spectrum AGNs find that the majority shows significant variability and that the number of these variable sources probably increases at low Galactic latitudes (e.g., Spangler et al. 1989; Ghosh & Rao 1992; Gaensler & Huntstead 2000; Ofek & Frail 2011). The source population in the flux density range of our survey is known to be dominated by AGNs and a significant fraction (∼50%) of these are compact, flat-spectrum AGNs and hence are expected to show short-term flux density variations (de Zotti et al. 2010).

8.2. Variability on Timescale of Years

By comparing our 2008 and 2010 catalogs, we were able to probe the variability of sources brighter than ≳0.5 mJy on two-year timescales. However, this comparison is limited to only two epochs. Each of the two epochs in our two year timescale variability analysis is composed of multiple epochs taken (≈δt) days to weeks apart. Therefore, in this analysis, short-term variability is averaged out. For example, at 5 GHz, variability due to scintillations will typically have a timescale shorter than a few days.

Figure 8 shows a comparison of the 2008 and 2010 peak flux densities for all radio sources in the Master catalog. Note that the 100 MHz difference in the center frequencies and the different bandwidths used (100 MHz versus 256 MHz) between the VLA (2008) and EVLA (2010) observations could lead to a systematic offset between the flux densities of the point sources in Figure 8. For a steep spectrum source (-1) the bias is of order 3%, and is smaller for flatter spectral indices. The dashed lines represent the mean noise 4σ and 8σ confidence variability contours. Based on χ^2_V (Table 6), we find 10 sources (2% of all the sources) which have variability with confidence level larger than about 4σ (i.e., $\chi^2_V > 16$, assuming one degree of freedom). These variable candidates are listed in Table 6 (below the horizontal line). We note that the χ^2_V calculation takes into account the gain correction factors and the cosmic errors described in Section 6. We visually inspected the images of all 10 variable candidates and verified that they are not sidelobe artifacts.

J213626.36+413926.6 is the only significant strong variable (i.e., with χ^2/dof $> 16/1$ and $V_F > 0.5$) in our two-year comparison. In 2010, it has a peak flux density (uncorrected for primary beam attenuation) of 627 ± 50 μJy (12.5σ), while in 2008 there is a nominal detection of the source at this position with a peak flux density of 197 ± 75 μJy (2.6σ). The source-specific flux was well below the detection threshold for every one of the 11 epochs in 2008 but it is visible in all five epochs in 2010. We note that this source is one of the two faint sources seen above the dashed line on the right side of Figure 4. For this reason, we do not classify this as a transient source but it appears instead to be a persistent radio source that has tripled its flux density over a two-year interval. There is no known cataloged source at this position in the NVSS catalog (Condon

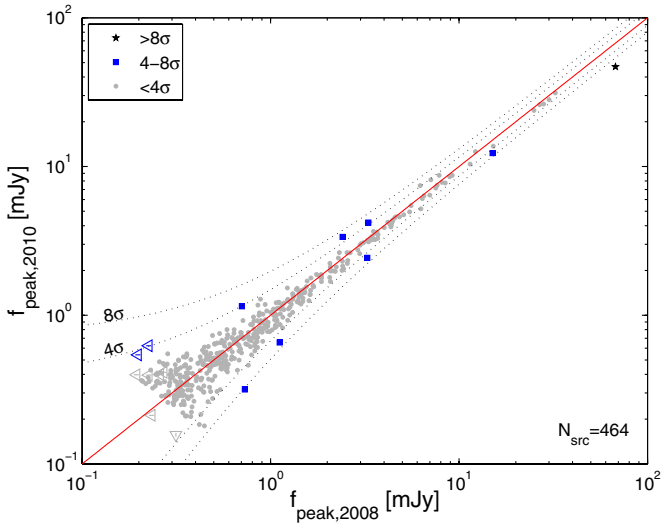

Figure 8. Comparison of the 2008 and 2010 peak flux densities for all radio sources in the Master catalog. The flux densities are not corrected for beam attenuation, but they are gain corrected (Section 6). Equal flux densities are indicated by a solid line. The dashed lines are the 4σ and 8σ confidence level contours based on the mean noise properties of the images and are calculated assuming that the noise has a constant component, which is the rms of the two yearly images (Table 4) added in quadrature with a specific flux-dependent component which is given by the cosmic errors discussed in Section 6. The average rms noise for the summed 2008 images was 72 μJy beam^{-1} and for 2010 images it was 56 μJy beam^{-1}. The shape and color coding represent χ^2 (one dof) of individual objects based on the actual noise rather than the average noise (see the legend). In cases where the measured flux density is lower than three times the rms noise, we mark the 3σ upper limit on the flux. These upper limits are marked by open triangles where the direction of the limit is given by the direction of the tip of the triangle (bottom or left) as well as the line inside the triangle (vertical or horizontal).

(A color version of this figure is available in the online journal.)

et al. 1998) nor in the SIMBAD or NED databases. A possible explanation for this source is that it is a radio supernova or some other kind of a transient (e.g., Nakar & Piran 2011) embedded in a faint resolved source.

Our Master catalog contains 317 sources brighter than J213626.36+413926.6. Therefore, we roughly estimate that the fraction of strong variables with two epochs $V_F > 0.5$ is $0.32^{+0.73}_{-0.26}$%. However, we note that this measurement is based on averaging out variability on timescales shorter than a few weeks.

9. DISCUSSION

We present a 16-epoch, Galactic plane survey for radio transients and variables at 5 GHz. We detected one possible transient and many variable sources. The transient areal density and rate based on this single detection are derived in Section 9.1. In Section 9.2 we discuss our variability study and compare it to previous surveys.

9.1. Transient Areal Density and Rate

The analysis of our data revealed a single radio transient candidate. The area encompassed within a single half-power beam (radius of $r_{\rm HP} = 4\farcm65$) in which we searched for transients is 0.00601 deg^2 and the area we targeted within the half-power radius of all 141 fields is 2.66 deg^2. Given that each field was observed on average 15.70 times (the sum of Column 4 in Table 2 divided by the number of fields), the total area covered by our survey over all the epochs is 41.2 deg^2. Our survey used an uncorrected peak flux density limit of 1.5 mJy for transients. However, the sensitivity within the field of view of a single beam imaging is not uniform and degrades by a factor of two at the half-power radius. In order to calculate the transient areal density from these parameters, we need to assume something about the source number count function. We parameterize the source number count function as a power law of the form

$$\kappa(>f) = \kappa_0 (f/f_0)^{-\alpha}, \quad (6)$$

where f is specific flux, $\kappa(> f)$ is the sky surface density of sources brighter than f, κ_0 is the sky surface density of sources brighter than f_0, and α is the power-law index of the source number count function. It is well known that for homogeneous source distribution in a Euclidean universe and arbitrary luminosity function $\alpha = 3/2$. In Appendix C, we derive a simple relation for the number of sources that are expected to be detected in a beam with a power sensitivity that falls like a Gaussian as a function of f_0, κ_0, α, $r_{\rm HP}$, the search radius $r_{\rm max}$, and the specific flux limit at the beam center $f_{\rm min,0}$.

Based on Equation (C5), and assuming $\alpha = 3/2$, we find that the transient areal density at 1.8 mJy (corrected for the CLEAN bias) is

$$\kappa(>1.8\,{\rm mJy}) = 0.039^{+0.13,+0.18}_{-0.032,-0.038}\,{\rm deg}^{-2}, \quad (7)$$

where the errors correspond to 1σ and 2σ confidence intervals, calculated using the prescription of Gehrels (1986). If our detected transient is not real then our survey poses a 95% confidence upper limit on the transient rate of $\kappa(>1.8\,{\rm mJy}) < 0.15$ deg^{-2}.

Translation of our areal density to transient rate depends on the transient duration $t_{\rm dur}$ and it is

$$\Re(>1.8\,{\rm mJy}) = \left(28^{+65,+132}_{-23,-27}\right)\left(\frac{t_{\rm dur}}{0.5\,{\rm day}}\right)^{-1}{\rm deg}^{-2}\,{\rm yr}^{-1}. \quad (8)$$

Note that this translation is correct only if $t_{\rm dur}$ is smaller than the time between epochs.

Figure 1 presents a summary of the radio transients and persistent sources areal density as observed by various searches and at different frequencies. This figure is largely based on Table 1 and the areal density reported here. As shown in this figure, the areal density derived in this work is roughly consistent with the expectation based on the Bower et al. (2007) transient sky surface density.

Moreover, it is roughly consistent with the sky surface density of the Nasu survey transients. We note that the Nasu sky surface density is based on our limited knowledge of this project (see Section 2). This comparison assumes that the transient areal density on the celestial sphere is uniform.

This figure implies that the areal density of radio transients in the sky is roughly 2–3 orders of magnitude below the persistent radio source sky surface density. This is in contrast to the visible light sky in which the fraction of transients (excluding solar system minor planets) among persistent sources is roughly 10^{-4} down to the limiting magnitude of surveys such as the Palomar Transient Factory (Law et al. 2009; Rau et al. 2009).

It is interesting to compare this figure to some recent predictions. Nakar & Piran (2011) predict that compact binary mergers, regardless of whether or not they are associated with short-duration gamma-ray bursts (e.g., Nakar 2007), will produce radio afterglows with a duration of several months. They suggest that the two-month-long radio transient RT19870422

detected by Bower et al. (2007) may be a binary merger radio afterglow. Moreover, they find that the rate inferred from this event is consistent with the predicted rate of binary merger events.

Giannios & Metzger (2011) suggest that tidal flare events may produce radio transients with durations of months to years, with a 5 GHz peak flux density of 1 mJy at a distance of 1 Gpc (i.e., $z \cong 0.2$). This idea is in agreement with recent observations (e.g., Levan et al. 2011). The total comoving volume[12] enclosed within a luminosity distance of 1 Gpc is 2.4×10^9 Mpc^3 or 5.9×10^4 Mpc^3 deg^{-2}. Bower et al. (2007) do not find any transients with a duration of two months, which are associated with the nucleus of a galaxy. This is translated to a 95% confidence upper limit on the rate of radio tidal flare events, brighter than 1 mJy, of $\sim$0.1 deg^{-2} yr^{-1}. Therefore, in the context of the Giannios & Metzger's (2011) predictions, we can put an upper limit of $\sim 7 \times 10^{-6}$ Mpc^3 yr^{-1} on the rate of tidal flare event radio afterglows. This is in rough agreement with the predicted tidal flares rate (Magorrian & Tremaine 1999; Wang & Merritt 2004).

Finally, we note that our detection rate is consistent with an old NS origin as suggested in Ofek et al. (2010), and with their expected surface density at low Galactic latitude based on the Ofek (2009) simulations.

9.2. Comparison of Variability with Previous Surveys

We analyzed the variability of the sources detected in our survey on days–weeks timescales and two-year period. On short timescales, we find that a considerable fraction of the bright point sources are variables. At the 10–100 mJy range, it seems that more than half the sources are variables on some level ($>4\sigma$). Furthermore, we find that 30% of the sources in our survey, which are brighter than $\approx$1.5 mJy, are variables (at the 4σ level). This is considerably higher than the fraction of variables reported in some other surveys (e.g., Gregory & Taylor 1986; de Vries et al. 2004; Becker et al. 2010). We suggest that a possible explanation for this apparent discrepancy is that the sources in these surveys were extracted in a way that washed out short timescale variability (see Section 8.1). This is supported by the fact that our two-year timescale variability study, in which each epoch is composed by averaging multiple observations, shows a smaller fraction of variables. Moreover, our structure function analysis shows that a large fraction of the variability component happens on timescales shorter than about a few days. Variability of compact radio sources on day timescales is known for a long time and was found by Heeschen (1982; 1984). Moreover, a large fraction of variable sources were previously reported by some other efforts, which did not average out short timescales variability (e.g., Lovell et al. 2008).

We speculate that the fast rise of the structure function on $\approx$10 day timescales is due to scintillations in the interstellar medium (ISM). These timescales are consistent with those expected theoretically from refractive scintillations at 5 GHz (e.g., Blandford et al. 1986; Hjellming & Narayan 1986). Moreover, similar rise times were reported by other efforts (e.g., Qian et al. 1995). Unlike diffractive scintillation which may produce strong variability on timescale of hours (StD/$\langle f \rangle$ of 80%; e.g., Goodman 1997; Frail et al. 2000), refractive scintillations can easily explain the observed amplitude of $\approx$13%. We note that a comparison of models with observations suggests that most of the radio source variability below 5 GHz is due to scintillations, while above 5 GHz there is an intrinsic variability component (e.g., Hughes et al. 1992; Mitchell et al. 1994; Qian et al. 1995). Therefore, we cannot rule out the possibility that some of the variability we detected in our survey is intrinsic to the sources.

After averaging out variations on timescale of days, our two-year variability analysis indicates that about 0.3% of the sources above 0.5 mJy are strong variables ($V_F > 0.5$ for $N_{\rm ep} = 2$), and that only a small fraction $\approx$3% of the sources are variables at some level. This finding supports the hypothesis that the main reason for low-amplitude radio variability at 5 GHz is due to scintillations.

It is suspected that the fraction of radio variable sources increases toward the Galactic plane (e.g., Spangler et al. 1989; Ghosh & Rao 1992; Gaensler & Hunstead 2000; Lovell et al. 2008; Becker et al. 2010; Ofek & Frail 2011), plausibly due to Galactic scintillations. However, there are some claims as yet unconfirmed that the number of *intrinsically* strong variables, at 5 GHz, increases toward the Galactic plane (Becker et al. 2010). Specifically, Becker et al. (2010) suggested that there is a separate Galactic population of *strong* variables. As noted in Section 2, they found that more than half of their variables, on timescales of years, varied by more than 50% in the 1–100 mJy flux density range. Moreover, they found that these strong variables were concentrated at low Galactic latitudes and toward the inner Galaxy. In contrast, we find a much smaller fraction of strong variables (see Section 8.2). However, Becker et al. (2010) observed sources within one degree of the Galactic plane, while our survey sampled Galactic latitudes $|b| \cong 6^\circ$–8°.

10. SUMMARY

We present a VLA 5 GHz survey to search for radio transients and explore radio variability in the Galactic plane. Our survey represents the first attempt to discover radio transients in near real-time and initiate multiwavelength follow-up. Our real-time search identified two possible transients. However, follow-up observations and our post-survey analysis showed that these candidates are not transient sources. Nevertheless, in one case, we were able to initiate visible light observations of the transient candidate field only one hour after the candidate was detected.

Our post-survey analysis reveals one possible transient source detected at the 5.8σ level. Our P60 images of this transient field, taken two days after the transient detection, do not reveal any visible light source brighter than i-band magnitude of 21 associated with the transient within $2''$. The transient has a timescale longer than one minute. However, we cannot put an upper limit on its duration since it was detected on the first epoch of our survey. Based on this single detection, we find an areal density of $\approx$0.04 deg^{-2} for transients brighter than 1.8 mJy. The transient surface density found in this paper is compared with other surveys in Figure 1. Our transient areal density is roughly consistent with the one reported by Bower et al. (2007), corrected for the flux density limit. This is also roughly consistent, up to a possible spectral correction factor, with the rates reported by Levinson et al. (2002) and Kida et al. (2008). Based on existing evidence, we cannot rule out the hypothesis that these transients, if real, are originating from Galactic isolated old NS (Ofek et al. 2010).

Finally, we present a comprehensive variability analysis of our data, with emphasis on proper calibration of the data and estimating systematic noise. Our findings suggest that short timescale variability among 5 GHz point sources is common.

[12] Assuming WMAP fifth-year cosmological parameters (Komatsu et al. 2009).

In fact, above 1.5 mJy at least 30% of the point sources are variables with variability exceeding our 4σ detection level. This is consistent with the Lovell et al.'s (2008) results and is plausibly explained by refractive scintillations in the ISM.

We are grateful to Barry Clark for his help with scheduling the VLA observations. We thank the anonymous referee for useful comments. E.O.O. is supported by an Einstein fellowship and NASA grants. Support for program number HST-GO-11104.01-A was provided by NASA through a grant from the Space Telescope Science Institute, which is operated by the Association of Universities for Research in Astronomy, Incorporated, under NASA contract NAS5-26555. A.G. acknowledges support by the Israeli Science Foundation, an EU Seventh Framework Programme Marie Curie IRG fellowship, the Benoziyo Center for Astrophysics, and the Yeda-Sela fund at the Weizmann Institute. This paper is based on observations conducted with the VLA, which is operated by the National Radio Astronomy Observatory (NRAO), a facility of the National Science Foundation operated under cooperative agreement by Associated Universities, Inc.

APPENDIX A

ESTIMATE OF THE GAIN CORRECTION FACTORS

In order to construct the best light curves of the sources, we need to remove any systematic factors influencing the measurements. A way to do this is to use the fact that the actual light curves of many sources are not correlated. Therefore, in the absence of systematic factors affecting the measurements, the scatter in the average light curve should be minimized. In order to minimize the scatter in the average light curve of our sources, we multiplied the flux densities at each epoch of observation (taken during ∼3 hr) by a "gain" correction factor, such that the residuals in all light curves, compared with a constant light curve, will be minimized. This problem is similar to producing relative photometry light curves in optical astronomy.

We used a linear least-squares minimization technique. Using this method, we are solving for the best zero-point normalization (per epoch) and the best "mean" flux density of each source that minimize the global scatter in all the light curves. This technique was already introduced by Honeycutt (1992) but here we write it in a more easy form to use and we also add a linear set of constraints for simultaneous absolute calibration.

We work in a "magnitude" system (i.e., $m = -2.5\log_{10} f$). One advantage of the magnitude system is that the error distribution (given by the logarithm of a Poisson error distribution) is, for small numbers, more symmetrical. This may be somewhat important for faint sources.[13] The basic idea of this technique is to simultaneously solve the following set of equations in the least-squares sense:

$$m_{ij} \cong z_i + \bar{m}_j, \tag{A1}$$

where m_{ij} is a $p \times q$ matrix that contains all the measured ("instrumental") magnitudes, i is the epoch index (p epochs), and j is the source index (q sources). Here, $\bar{m}_j$ is the mean magnitude of the jth source and z_i is the zero point of the ith epoch. We note that $\bar{m}_j$ and z_i are free parameters. In case we have error measurements, let σ_{ij}^m be the respective errors in the instrumental magnitudes. In some cases, we may have additional constraints such as the calibrated magnitudes, M_j (and respective errors, σ_j^M), of some or all the sources. This additional information can be used as constraints on the system of linear equations. Using these constraints, our output magnitudes will be calibrated with respect to a set of reference sources.

Given m_{ij} and σ_{ij}^m, and the optional M_j and σ_j^M, we would like to find the properly weighted best-fit free parameters z_i and $\bar{m}_j$. Let $\vec{m}$ be a vector of the observable quantities, and $\vec{\sigma}$ be the respective vector of errors in these quantities obtained by rearranging the matrices of instrumental and calibrated magnitudes (i.e., m_{ij} and σ_{ij}^m):

$$\vec{m} = \begin{bmatrix} m_{11} \\ m_{12} \\ \vdots \\ m_{1q} \\ \hline m_{21} \\ m_{22} \\ \vdots \\ m_{2q} \\ \hline \vdots \\ \hline m_{p1} \\ m_{p2} \\ \vdots \\ m_{pq} \\ \hline\hline M_1 \\ M_2 \\ \vdots \\ M_q \end{bmatrix}, \quad \vec{\sigma} = \begin{bmatrix} \sigma_{11}^m \\ \sigma_{12}^m \\ \vdots \\ \sigma_{1q}^m \\ \hline \sigma_{21}^m \\ \sigma_{22}^m \\ \vdots \\ \sigma_{2q}^m \\ \hline \vdots \\ \hline \sigma_{p1}^m \\ \sigma_{p2}^m \\ \vdots \\ \sigma_{pq}^m \\ \hline\hline \sigma_1^M \\ \sigma_2^M \\ \vdots \\ \sigma_q^M \end{bmatrix}. \tag{A2}$$

Note that the elements below the double horizontal lines are optional elements, needed only if we want to simultaneously apply a magnitude calibration.

Next, we can define a vector of free parameters we would like to fit:

$$\vec{P} = [z_1\, z_2 \ldots z_p\,,\ \bar{m}_1\, \bar{m}_2 \ldots \bar{m}_q]^T, \tag{A3}$$

where the superscript T indicates a transpose operator. In that case, the design matrix H, which satisfies $\vec{m} \cong H\vec{P}$, is easy to construct:

$$H = \left[\begin{array}{c|c} I_{j=1}^{q\times p} & I^{q\times q} \\ \hline I_{j=2}^{q\times p} & I^{q\times q} \\ \hline \vdots & I^{q\times q} \\ \hline I_{j=q}^{q\times p} & I^{q\times q} \\ \hline\hline 0^{q\times p} & I^{q\times q} \end{array}\right], \tag{A4}$$

where $I_{j=k}^{q\times p}$, is a $q \times p$ matrix in which the kth column contains ones, while the rest of the elements are zeros, $I^{q\times q}$ is a $q \times q$ identity matrix, and $0^{q\times p}$ is a $q \times p$ zeros matrix.

Note that (again) the lower block of the matrix H, separated by two horizontal lines, is an optional section that is used for the magnitude zero-point calibration. This additional section acts like constraints on the system of linear equations.

[13] For example, the Poisson 1σ confidence interval for one event is from 1/5.79 to 3.30. The degree of asymmetry here is 1.75 (= 5.79/3.30). While the same confidence interval in $\log_{10}$-space is from −0.76 to 0.52, the asymmetry is ≈1.5 (= 0.76/0.52).

Table 8
Translation of $\langle V_R \rangle$ to StD/$\langle f \rangle$

StD/$\langle f \rangle$	0.01	0.05	0.10	0.15	0.20	0.25	0.31	0.35	0.38	0.42	0.43	0.44	0.45	0.46	0.47	0.48	0.50	0.51
$S_{\log N}$	0.01	0.05	0.10	0.15	0.20	0.25	0.30	0.34	0.37	0.40	0.41	0.42	0.43	0.44	0.45	0.46	0.47	0.48
$N_{\rm ep}$																		
2	1.01	1.06	1.12	1.19	1.27	1.36	1.45	1.54	1.60	1.68	1.70	1.73	1.75	1.78	1.81	1.83	1.86	1.89
3	1.02	1.09	1.19	1.30	1.43	1.57	1.72	1.87	1.98	2.11	2.15	2.20	2.24	2.29	2.34	2.39	2.44	2.49
4	1.02	1.11	1.23	1.37	1.53	1.72	1.92	2.11	2.27	2.43	2.49	2.55	2.62	2.68	2.75	2.81	2.88	2.96
5	1.02	1.12	1.27	1.43	1.62	1.83	2.08	2.31	2.50	2.70	2.77	2.85	2.92	3.00	3.09	3.17	3.26	3.35
6	1.03	1.14	1.29	1.47	1.69	1.93	2.21	2.47	2.69	2.93	3.01	3.10	3.19	3.28	3.38	3.48	3.58	3.68
7	1.03	1.15	1.32	1.51	1.74	2.01	2.32	2.61	2.86	3.13	3.22	3.32	3.42	3.53	3.64	3.75	3.87	3.98
8	1.03	1.15	1.33	1.54	1.79	2.08	2.42	2.74	3.01	3.31	3.41	3.52	3.63	3.74	3.87	3.99	4.12	4.26
9	1.03	1.16	1.35	1.57	1.84	2.15	2.51	2.86	3.14	3.46	3.58	3.70	3.82	3.95	4.08	4.22	4.36	4.50
10	1.03	1.17	1.36	1.60	1.87	2.20	2.59	2.96	3.27	3.61	3.74	3.86	3.99	4.13	4.28	4.42	4.57	4.73
11	1.03	1.17	1.38	1.62	1.91	2.26	2.66	3.05	3.38	3.75	3.88	4.01	4.15	4.30	4.45	4.61	4.77	4.94
12	1.03	1.18	1.39	1.64	1.94	2.30	2.73	3.14	3.49	3.87	4.01	4.16	4.31	4.46	4.62	4.79	4.96	5.14
13	1.03	1.18	1.40	1.66	1.97	2.35	2.80	3.22	3.58	3.99	4.13	4.29	4.45	4.61	4.78	4.96	5.14	5.33
14	1.03	1.19	1.41	1.68	2.00	2.39	2.86	3.30	3.68	4.10	4.25	4.41	4.58	4.75	4.93	5.12	5.31	5.50
15	1.04	1.19	1.42	1.69	2.03	2.43	2.91	3.37	3.76	4.21	4.36	4.53	4.70	4.88	5.07	5.27	5.47	5.68
16	1.04	1.19	1.43	1.71	2.05	2.46	2.96	3.44	3.84	4.30	4.47	4.64	4.82	5.01	5.20	5.41	5.62	5.83
17	1.04	1.20	1.44	1.72	2.07	2.50	3.01	3.50	3.92	4.40	4.57	4.75	4.93	5.13	5.33	5.54	5.76	5.99
18	1.04	1.20	1.44	1.74	2.09	2.53	3.06	3.56	4.00	4.49	4.67	4.85	5.04	5.24	5.45	5.67	5.90	6.13
19	1.04	1.20	1.45	1.75	2.11	2.56	3.10	3.62	4.07	4.58	4.76	4.95	5.15	5.35	5.57	5.79	6.03	6.27
20	1.04	1.21	1.46	1.76	2.13	2.59	3.14	3.67	4.13	4.66	4.85	5.04	5.24	5.46	5.68	5.91	6.16	6.41

The rank of the matrix H without the lower block is $p+q-1$. This is because without the calibration block there is an arbitrariness in adding a zero point to each epoch. Adding the calibration block (or part of it) fixes this problem and in that case the rank of H is $p+q$. In cases where a given source does not appear in a specific epoch, we simply have to remove the appropriate row in H, $\vec{m}$, and $\vec{\sigma}$.

In order to find the best-fit parameters $\vec{P}$ and their respective errors σ^P, we need to find $\vec{P}$ that minimizes χ^2:

$$\chi^2 = (\vec{m} - H\vec{P})^T \left[\sigma_{ij}^2\right]^{-1} (\vec{m} - H\vec{P}), \qquad \text{(A5)}$$

where $[\sigma_{ij}^2]$ is the matrix of measurement errors σ_{ij}^m. The problem of finding $\vec{P}$ and their corresponding errors is described in many textbooks (e.g., Press et al. 1992; for a tutorial, see Gould 2003).

The design matrix, H, even without the magnitude calibration part, is a $(p \times q) \times (p+q)$ matrix. For many problems, the matrix H may be huge and requires a lot of computer memory. However, H is highly sparse, and therefore sparse matrix implementations can be used if needed. Alternatively, this can be solved using the conjugate gradient method.[14]

We note that in practice this method may be applied iteratively. After the first iteration, we can check χ_j^2 for each source and χ_i^2 for each epoch. Then, we can remove sources with large values of χ_j^2, and/or we can add a "cosmic" error to all the measurements in an epoch with large χ_i^2. After constructing the new H and Y, we may apply the inversion again.

We note that typically, in addition to σ_{ij}^m (the errors associated with the individual sources), there are additional errors (e.g., calibration errors in radio astronomy and flat-fielding errors in optical astronomy). Ignoring these errors is not recommended since it will give over weight to sources with small errors. A solution to this problem is, again, to apply this method in iterations. After the first iteration it is possible to estimate the cosmic error term (based on the residuals from the best fit), and to add these cosmic errors to the instrumental errors in the second iteration.

Finally, using this method, additional de-trending is possible. For example, one can add additional columns to the design matrix (and corresponding additional terms to the vector of free parameters) that represent changes in the zero point as a function of additional parameters. For example, in radio astronomy, this may be a variation in the zero point as a function of the distance from the beam center, and in optical astronomy this may be an airmass–color term, positional terms, color terms affecting different instruments, and more.

APPENDIX B

V_R AND V_F STATISTICS

The V_R and V_F defined in Equations (3) and (4) are sensitive to the number of measurements. This complicates the comparison between surveys with different numbers of epochs. In order to demonstrate this and to provide a method to roughly convert these variability indicators between different surveys, here we calculate the expectation value for V_R as a function of the number of epochs in a survey, $N_{\rm ep}$, and the StD/$\langle f \rangle$ of a source light curve. We note that V_R and V_F are exchangeable.

In order to calculate this conversion, we performed the following simulations. We generated random light curves with $N_{\rm ep}$ points and which are drawn from a log-normal standard deviation, $S_{\log N}$. For each value of $N_{\rm ep}$ and $S_{\log N}$, 10^6 light curves were generated, and StD/$\langle f \rangle$ and $\langle V_R \rangle$ were calculated. In Table 8, we list the V_R expectation values as a function of $N_{\rm ep}$ (rows) and StD/$\langle f \rangle$ (columns). Below the StD/$\langle f \rangle$, we also give the appropriate $S_{\log N}$.

APPENDIX C

ESTIMATE OF THE AREAL DENSITY IN A NON-UNIFORM BEAM

Typically, the sensitivity of a radio telescope is not uniform across its field of view and depends on the radial angular distance

[14] See basic description and overview in http://www.cs.cmu.edu/~quake-papers/painless-conjugate-gradient.pdf.

from the beam center. In order to convert the areal density, κ_0, of sources brighter than the flux density f_0, to the expected number of detectable events by a radio telescope, we need to take into account the beam pattern and the source number count function.

We parameterize the cumulative density of events as a function of flux density as a power law

$$\kappa(>f) \equiv \int_f^{\infty} \kappa(f)\,df = \kappa_0 (f/f_0)^{-\alpha}, \quad \text{(C1)}$$

where $\kappa(f)df$ is the number of sources per flux density interval, and α is the power-law index of the source number count function. For a uniform density population with arbitrary luminosity function in a Euclidean universe $\alpha = 3/2$.

The number of sources that can be detected in a single beam in a single epoch up to an angular distance $r_{\max}$ from the beam center is

$$\begin{aligned} N_b &= \int_0^{r_{\max}} 2\pi r dr \int_{f_{\min}(r)}^{\infty} \kappa(f)\,df \\ &= \int_0^{r_{\max}} 2\pi r \kappa_0 [f_{\min}(r)/f_0]^{-\alpha} dr, \end{aligned} \quad \text{(C2)}$$

where r is the distance from the beam center, f is the flux density, and $f_{\min}(r)$ is the detection threshold as a function of angular distance r. For convenience, we will assume that the beam pattern is Gaussian so that

$$f_{\min}(r) = f_{\min,0} e^{+r^2 \ln 2/(r_{\rm HP}^2)}, \quad \text{(C3)}$$

where $r_{\rm HP}$ is the half-width at half-power,[15] and $f_{\min,0}$ is the detection limit at the beam center (i.e., $r = 0$).

In the case of $\alpha = 3/2$ and a Gaussian beam pattern, the integral in Equation (C2) has an analytic solution

$$N_{\rm b}(\alpha = 3/2) = -\frac{2\pi\kappa_0 r_{\rm HP}^2}{3\ln 2}\left[\frac{f_{\min,0}}{f_0} e^{+r^2 \ln 2/r_{\rm HP}^2}\right]^{-3/2}\Bigg|_0^{r_{\max}}. \quad \text{(C4)}$$

For other values of α, this integral can be evaluated numerically. Rearranging Equation (C4), the surface density, assuming $\alpha = 3/2$, is given by

$$\kappa_0 = \frac{3N_b \ln 2}{2\pi r_{\rm HP}^2}\left(\frac{f_{\min,0}}{f_0}\right)^{3/2}\left(1 - e^{-3r_{\max}^2 \ln 2/(2r_{\rm HP}^2)}\right)^{-1}. \quad \text{(C5)}$$

Finally, the ratio between $\pi r_{\max}^2$ and $N(\alpha = 3/2; r_{\max})$ gives the correction factor of 1.61 we used in Section 2.

REFERENCES

Backer, D. C., Kulkarni, S. R., Heiles, C., Davis, M. M., & Goss, W. M. 1982, Nature, 300, 615
Bannister, K., Murphy, T., Gaensler, B. M., Hunstead, R., & Chatterjee, S. 2011, MNRAS, 412, 634
Becker, R. H., Helfand, D. J., White, R. L., & Proctor, D. D. 2010, AJ, 140, 157
Becker, R. H., White, R. L., & Edwards, A. L. 1991, ApJS, 75, 1
Becker, R. H., White, R. L., & Helfand, D. J. 1995, ApJ, 450, 559
Bell, M. E., Fender, R. P., Swinbank, J., et al. 2011, MNRAS, 415, 2
Blandford, R., Narayan, R., & Romani, R. W. 1986, ApJ, 301, L53
Bower, G. C., Croft, S., Keating, G., et al. 2010, ApJ, 725, 1792
Bower, G. C., & Saul, D. 2011, ApJ, 728, L14
Bower, G. C., Saul, D., Bloom, J. S., et al. 2007, ApJ, 666, 346
Carilli, C. L., Ivison, R. J., & Frail, D. A. 2003, ApJ, 590, 192
Cenko, S. B., Fox, D. B., Moon, D.-S., et al. 2006, PASP, 118, 1396
Condon, J. J. 1984, ApJ, 287, 461
Condon, J. J., Broderick, J. J., & Seielstad, G. A. 1989, AJ, 97, 1064
Condon, J. J., Broderick, J. J., Seielstad, G. A., Douglas, K., & Gregory, P. C. 1994, AJ, 107, 1829
Condon, J. J., Cotton, W. D., Greisen, E. W., et al. 1998, AJ, 115, 1693
Croft, S., Bower, G. C., Ackermann, R., et al. 2010, ApJ, 719, 45
Croft, S., Bower, G. C., Keating, G., et al. 2011, ApJ, 731, 34
de Vries, W. H., Becker, R. H., White, R. L., & Helfand, D. J. 2004, AJ, 127, 2565
de Zotti, G., Massardi, M., Negrello, M., & Wall, J. 2010, A&AR, 18, 1
Dent, W. A. 1965, Science, 148, 1458
Edelson, R. A., & Krolik, J. H. 1988, ApJ, 333, 646
Efron, B. 1982, CBMS-NSF Regional Conference Series in Applied Mathematics (Philadelphia, PA: SIAM)
Efron, B., & Tibshirani, R. J. 1993, An Introduction to the Bootstrap (Monographs on Statistics and Applied Probability, Vol. 57; London: Chapman & Hall)
Fiedler, R. L., Dennison, B., Johnston, K. J., & Hewish, A. 1987, Nature, 326, 675
Frail, D. A., Kulkarni, S. R., Berger, E., & Wieringa, M. H. 2003, AJ, 125, 2299
Frail, D. A., Kulkarni, S. R., Costa, E., et al. 1997, ApJ, 483, L91
Frail, D. A., Kulkarni, S. R., Hurley, K. C., et al. 1994, ApJ, 437, L43
Frail, D. A., Waxman, E., & Kulkarni, S. R. 2000, ApJ, 537, 191
Gaensler, B. M., & Hunstead, R. W. 2000, PASA, 17, 72
Gal-Yam, A., Ofek, E. O., Poznanski, D., et al. 2006, ApJ, 639, 331
Gehrels, N. 1986, ApJ, 303, 336
Gehrels, N., Chincarini, G., Giommi, P., et al. 2004, ApJ, 611, 1005
Ghosh, T., & Rao, A. P. 1992, A&A, 264, 203
Giannios, D., & Metzger, B. D. 2011, MNRAS, 1137
Goodman, J. 1997, New Astron., 2, 449
Goodman, J. J., Romani, R. W., Blandford, R. D., & Narayan, R. 1987, MNRAS, 229, 73
Gould, A. 2003, arXiv:astro-ph/0310577
Green, D. A. 2002, VizieR Online Data Catalog, 7227
Gregory, P. C., Capak, P., Gasson, D., & Scott, W. K. 2001, in IAU Symp. 205, Galaxies and Their Constituents at the Highest Angular Resolutions, ed. R. T. Schilizzi (Cambridge: Cambridge Univ. Press), 98
Gregory, P. C., Scott, W. K., Douglas, K., & Condon, J. J. 1996, ApJS, 103, 427
Gregory, P. C., & Taylor, A. R. 1978, Nature, 272, 704
Gregory, P. C., & Taylor, A. R. 1986, AJ, 92, 371
Heeschen, D. 1982, Proc. Symp. on Extragalactic Radio Sources 97, ed. D. S. Heeschen & C. M. Wade (Dordrecht: Reidel), 327
Heeschen, D. S. 1984, AJ, 89, 1111
Helfand, D. J., Becker, R. H., White, R. L., Fallon, A., & Tuttle, S. 2006, AJ, 131, 2525
Hewish, A., Bell, S. J., Pilkington, J. D. H., Scott, P. F., & Collins, R. A. 1968, Nature, 217, 709
Hjellming, R. M., & Narayan, R. 1986, ApJ, 310, 768
Honeycutt, R. K. 1992, PASP, 104, 435
Hughes, P. A., Aller, H. D., & Aller, M. F. 1992, ApJ, 396, 469
Hyman, S. D., Lazio, T. J. W., Kassim, N. E., et al. 2005, Nature, 434, 50
Kida, S., Niinuma, K., Suzuki, S., et al. 2008, New Astron., 13, 519
Komatsu, E., Dunkley, J., Nolta, M. R., et al. 2009, ApJS, 180, 330
Kuniyoshi, M., Daishido, T., Asuma, K., et al. 2006, PASP, 118, 901
Law, N. M., Kulkarni, S. R., Dekany, R. G., et al. 2009, PASP, 121, 1395
Levan, A. J., Tanvir, N. R., Cenko, S. B., et al. 2011, Science, 333, 199
Levinson, A., Ofek, E. O., Waxman, E., & Gal-Yam, A. 2002, ApJ, 576, 923
Lorimer, D. R., Bailes, M., McLaughlin, M. A., Narkevic, D. J., & Crawford, F. 2007, Science, 318, 777
Lovell, J. E. J., Rickett, B. J., Macquart, J.-P., et al. 2008, ApJ, 689, 108
Magorrian, J., & Tremaine, S. 1999, MNRAS, 309, 447
Matsumura, N., Daishido, T., Kuniyoshi, M., et al. 2007, AJ, 133, 1441
Matsumura, N., Niinuma, K., Kuniyoshi, M., et al. 2009, AJ, 138, 787
McLaughlin, M. A., Lyne, A. G., Lorimer, D. R., et al. 2006, Nature, 439, 817
Mitchell, K. J., Dennison, B., Condon, J. J., et al. 1994, ApJS, 93, 441
Monet, D. G., Levine, S. E., Canzian, B., et al. 2003, AJ, 125, 984
Murphy, T., Mauch, T., Green, A., et al. 2007, MNRAS, 382, 382
Nakar, E. 2007, Phys. Rep., 442, 166
Nakar, E., & Piran, T. 2011, arXiv:1102.1020
Niinuma, K., Asuma, K., Kuniyoshi, M., et al. 2007, ApJ, 657, L37
Ofek, E. O. 2009, PASP, 121, 814
Ofek, E. O., Breslauer, B., Gal-Yam, A., et al. 2010, ApJ, 711, 517
Ofek, E. O., & Frail, D. A. 2011, ApJ, 737, 45
Press, W. H., Teukolsky, S. A., Vetterling, W. T., & Flannery, B. P. 1992, Numerical Recipes in FORTRAN: The Art of Scientific Computing (2nd ed.; Cambridge: Cambridge Univ. Press)

[15] Related to σ of the Gaussian by $r_{\rm HP} = \sigma\sqrt{2\ln 2}$.

Qian, S. J., Britzen, S., Witzel, A. K., et al. 1995, A&A, 295, 47
Rau, A., Kulkarni, S. R., Law, N. M., et al. 2009, PASP, 121, 1334
Rees, M. J. 1967, MNRAS, 137, 429
Rickett, B. J. 1990, ARA&A, 28, 561
Scott, W. K. 1996, PhD thesis, Univ. British Columbia
Skrutskie, M. F., Cutri, R. M., Stiening, R., et al. 2006, AJ, 131, 1163
Spangler, S., Fanti, R., Gregorini, L., & Padrielli, L. 1989, A&A, 209, 315
Taylor, A. R., & Gregory, P. C. 1983, AJ, 88, 1784
Tsutsumi, T., Gregory, P. C., Duric, N., & Taylor, A. R. 1995, AJ, 110, 238
Wang, J., & Merritt, D. 2004, ApJ, 600, 149
Windhorst, R. A., Miley, G. K., Owen, F. N., Kron, R. G., & Koo, D. C. 1985, ApJ, 289, 494